

Radiative Weak Decays of Charm Mesons

Gustavo Burdman^(a), Eugene Golowich^(b)
JoAnne L. Hewett^(c) and Sandip Pakvasa^(d)

^(a)Fermilab

Batavia, IL 60510, USA

^(b)Department of Physics and Astronomy

University of Massachusetts, Amherst MA 01003, USA

^(c)Stanford Linear Accelerator Center

Stanford CA 94309, USA

^(d)Department of Physics and Astronomy

University of Hawaii, Honolulu HI 96822, USA

Abstract

We address Standard Model predictions for flavor-changing radiative transitions of the pseudoscalar charm mesons. Short-distance contributions in D radiative transitions are contrasted with those in B decays. A full analysis is presented of the $c \rightarrow u + \gamma$ electromagnetic penguin amplitude with QCD radiative corrections included. Given the importance of long-range effects for the charm sector, special attention is paid to such contributions as the vector dominance and pole amplitudes. A number of two-body final states in exclusive charm radiative decays is considered and the corresponding branching ratio predictions are given.

1 Introduction

Important milestones in the study of the b -quark system were reached with the recent observations of both the exclusive decay $B \rightarrow K^*\gamma$ ^[1]

$$B_{B \rightarrow K^*\gamma} = (4.5 \pm 1.5 \pm 0.9) \times 10^{-5} \quad , \quad (1)$$

and of the inclusive transition^[2]

$$B_{b \rightarrow s\gamma} = (2.32 \pm 0.57 \pm 0.35) \times 10^{-4} \quad . \quad (2)$$

To first approximation, these flavor-changing radiative decays can be interpreted at the quark level in terms of the $b \rightarrow s\gamma$ transition. The Standard Model allows for such a process by means of a one-loop penguin-type amplitude. Within errors, agreement of the measured branching ratios and Standard Model predictions appears to be reasonable. The small magnitudes of these branching ratios indicate just how sensitive experimental probes of b -quark hadrons have become. However, an outstanding question is the size of the long distance contributions^[3, 4] to such radiative B decays relative to the short distance penguin amplitude. This issue must be addressed in order to establish the viability of determining the value of the ratio of CKM matrix elements, $|V_{td}|/|V_{ts}|$, from a measurement of the ratio of exclusive branching fractions $B_{B \rightarrow \rho\gamma}/B_{B \rightarrow K^*\gamma}$.

Important as they are, the above measurements by no means exhaust the set of interesting problems. It has become increasingly evident that the database for charm hadrons is also in a state of rapid expansion, and that physically important levels of sensitivity are being achieved. Perhaps the most impressive example of this to-date is the recent observation of the nonleptonic decay $D^0 \rightarrow K^+\pi^-$, with branching ratio^[5]

$$\frac{B_{D^0 \rightarrow K^+\pi^-}}{B_{D^0 \rightarrow K^-\pi^+}} = 0.0077 \pm 0.0025 \pm 0.0025 \quad . \quad (3)$$

This transition has been interpreted as evidence of a doubly Cabibbo suppressed transition rather than of D^0 - \bar{D}^0 mixing.

The discussion in this paper will be directed towards a somewhat different aspect of charm physics, the flavor-changing radiative decays. These transitions require the joint occurrence of weak and electromagnetic interactions. From Table 1^{[6],[7],[8]}, we see that no such events (involving emission of real

or virtual photons) have yet been observed. However, these decays are an active area of study, and data gathered in ongoing fixed-target experiments are establishing markedly improved bounds. Our objective in the analysis to follow will be to provide up-to-date predictions for flavor-changing radiative transitions of charm systems. Since the experimental situation for charm mesons is at present more favorable than for charm baryons, we shall restrict our attention to the former. Even with this restriction, it is a tall order to supply accurate theoretical values. It has become evident over a long period of time that theoretical calculations of D -meson weak decays are not particularly trustworthy, due in part to the absence of a rapidly convergent approximation scheme and also to the presence of significant hadron dynamical effects in the D meson mass region. Despite this, we feel that one can make some definite statements, such as the relative importance of long-range and short-range effects and of the various types of final states which can reasonably be anticipated. We shall base our analysis on a variety of theoretical techniques, from operator-product expansion and renormalization-group methods to more phenomenological approaches like vector-meson-dominance (VMD). Measurement of radiative charm decays would probe the long distance contributions and thus provide further insight in the extrapolation of calculational techniques to the B sector.

Table 1 Status of Electroweak-induced Charm Decays

Mode	Branching Ratio
$D^0 \rightarrow \rho^0 \gamma$	$< 1.4 \times 10^{-4}$
$D^0 \rightarrow \phi^0 \gamma$	$< 2.0 \times 10^{-4}$
$D^0 \rightarrow \bar{K}^0 e^+ e^-$	$< 1.7 \times 10^{-3}$
$D^0 \rightarrow \rho^0 e^+ e^-$	$< 4.5 \times 10^{-4}$
$D^0 \rightarrow \rho^0 \mu^+ \mu^-$	$< 8.1 \times 10^{-4}$
$D^+ \rightarrow \pi^+ e^+ e^-$	$< 2.5 \times 10^{-3}$
$D^+ \rightarrow \pi^+ \mu^+ \mu^-$	$< 2.9 \times 10^{-3}$
$D^+ \rightarrow K^+ e^+ e^-$	$< 4.8 \times 10^{-3}$
$D^+ \rightarrow K^+ \mu^+ \mu^-$	$< 9.2 \times 10^{-3}$

Let us summarize the contents to follow. In Section 2, we consider the short-range component in radiative charm decays, primarily the charm counterpart of the penguin amplitude which dominates the radiative B -meson

decays. In addition to addressing c -quark physics, our analysis contains a purely theoretical advance by removing an unnecessary assumption made in earlier studies involving b -quark applications. Section 3 begins our analysis of the so-called ‘long-distance’ contributions with an analysis of pole diagrams, which are induced by the weak mixing of pseudoscalar and/or vector charm mesons with noncharm states. In Section 4, we continue our study of long distance effects by turning our attention to a study of VMD amplitudes. Our conclusions and recommendations for future studies are given in Section 5. There is also an Appendix in which the applicability of VMD to certain light-meson decays is commented on.

2 Short Distance Contributions

Examples of diagrams which mediate the short-distance transition amplitudes for radiative charm decay are depicted in Fig. 1. They have in common that the photon emission occurs in a region of spacetime determined by the propagator of the W -boson. In view of the large W -mass M_W , this region has a very limited extent compared to the length scale of the strong interactions, hence the name ‘short-distance’. Looking ahead, our conclusion regarding such short-distance amplitudes will be that in radiative decays of charm mesons they are small relative to long-distance effects, even though they receive large enhancements from QCD corrections. As described earlier, this is of course in stark contrast to B decay.

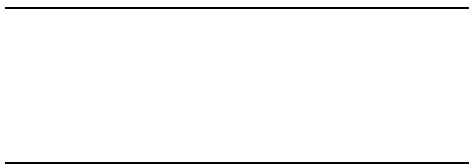


Figure 1. Short-distance Effects

In recognition of the importance attached to the electromagnetic penguin transition in radiative B decays, we give a brief pedagogical comparison

between the role played by this effect for B and for D decay. The two transitions in question are given at the quark-level by

$$\begin{aligned} b(\mathbf{p}, \lambda) &\rightarrow s(\mathbf{p}', \lambda') + \gamma(\mathbf{q}, \sigma) \\ c(\mathbf{p}, \lambda) &\rightarrow u(\mathbf{p}', \lambda') + \gamma(\mathbf{q}, \sigma) . \end{aligned} \quad (4)$$

To highlight the crucial role played by the quark masses and CKM matrix elements, let us at first ignore the effect of QCD radiative corrections. The relevant Feynman diagrams are then depicted in Figs. 1(a),1(c) and the penguin amplitude for the transition of a heavy quark Q to a much lighter quark q and an on-shell photon is given by^[9]

$$\begin{aligned} \mathcal{A}_{Q \rightarrow q\gamma}^{(\text{EM peng})} = & \quad (5) \\ & \frac{eG_F}{4\sqrt{2}\pi^2} \sum_i \lambda_i F_2(x_i) \bar{u}_q(p', \lambda') \epsilon^{\mu\dagger}(q, \lambda) \sigma_{\mu\nu} q^\nu [m_Q P_R + m_q P_L] u_Q(p, \lambda) , \end{aligned}$$

where $P_{R(L)}$ are the right(left)-handed helicity projection operators, $x_i \equiv m_i^2/M_W^2$, $\lambda_i \equiv V_{is}^* V_{ib}$ for $\mathcal{A}_{b \rightarrow s\gamma}$ and $\lambda_i \equiv V_{ci}^* V_{ui}$ for $\mathcal{A}_{c \rightarrow u\gamma}$. The function F_2 gives the contribution of each internal quark to the electromagnetic penguin loop,

$$F_2(x) = Q \left[\frac{x^3 - 5x^2 - 2x}{4(x-1)^3} + \frac{3x^2 \ln x}{2(x-1)^4} \right] + \frac{2x^3 + 5x^2 - x}{4(x-1)^3} - \frac{3x^3 \ln x}{2(x-1)^4} , \quad (6)$$

with Q being the charge of the internal quark. For $b \rightarrow s\gamma$ the sum is carried out over the quarks u, c, t and the term proportional to the s -quark mass in Eq. (5) is generally neglected, whereas for $c \rightarrow u\gamma$, one sums over the quarks d, s, b and ignores the corresponding term proportional to the u -quark mass.

Let us get acquainted with some of the numerical values. In Table 2, we first display the magnitude of the function F_2 and then fold in the CKM dependence for the $b \rightarrow s\gamma$ transition (we take $m_u = 5$ MeV, $m_c = 1.5$ GeV, $m_t = 174$ GeV, and the central values of the CKM matrix elements as given in Ref. [6]).

Table 2 Contributions to $b \rightarrow s + \gamma$

Quark	F_2	$ V_{ib} V_{is}^* F_2$
u	2.27×10^{-9}	1.29×10^{-12}
c	2.03×10^{-4}	7.34×10^{-6}
t	0.39	1.56×10^{-2}

Dominance of the t -quark intermediate state is evident, even upon including the CKM factors. Its effect is so large that the other intermediate states are numerically negligible and hence are typically omitted. The corresponding situation is given for $c \rightarrow u\gamma$ in Table 3 (with $m_d = 11$ MeV, $m_s = 150$ MeV, and $m_b = 4.9$ GeV).

Table 3 Contributions to $c \rightarrow u + \gamma$

Quark	F_2	$ V_{ci}^*V_{ui} F_2$
d	1.57×10^{-9}	3.36×10^{-10}
s	2.92×10^{-7}	6.26×10^{-8}
b	3.31×10^{-4}	3.17×10^{-8}

The amplitude for $c \rightarrow u\gamma$ differs from that of $b \rightarrow s\gamma$ in two important respects, (i) there is no single intermediate state which dominates, and (ii) the overall magnitude is much smaller.

Neglecting the final state fermion mass, the QCD uncorrected decay rate $\Gamma_{Q \rightarrow q\gamma}^{(0)}$ is given by

$$\Gamma_{Q \rightarrow q\gamma}^{(0)} = \frac{\alpha G_F^2}{128\pi^4} m_Q^5 \left| \sum_i \lambda_i F_2(x_i) \right|^2. \quad (7)$$

To obtain the branching fraction, the inclusive rate is scaled to that of the semi-leptonic decay $Q \rightarrow q'\ell\nu$. This procedure removes uncertainties in the calculation due to the overall factor of m_Q^5 which appears in both expressions, and reduces the ambiguities involved with the imprecisely determined CKM factors. Taking the above numerical values for the internal quark masses, and using the values of the semi-leptonic branching ratios as given in Ref. [6], this yields

$$\begin{aligned} B_{b \rightarrow s\gamma} &= \frac{3\alpha}{2\pi} \cdot \frac{|V_{tb}V_{ts}^*F_2(x_t)|^2}{|V_{cb}|^2 \left[g(m_c/m_b) + \frac{|V_{ub}|^2}{|V_{cb}|^2} g(m_u/m_b) \right]} \cdot B_{B \rightarrow X\ell\nu}, \\ &= 1.29 \times 10^{-4}, \\ B_{c \rightarrow u\gamma} &= \frac{3\alpha}{2\pi} \cdot \frac{|V_{cs}^*V_{us}F_2(x_s) + V_{cb}^*V_{ub}F_2(x_b)|^2}{|V_{cs}|^2 \left[g(m_s/m_c) + \frac{|V_{cd}|^2}{|V_{cs}|^2} g(m_d/m_c) \right]} \cdot B_{D^+ \rightarrow X\ell^+\nu}, \end{aligned} \quad (8)$$

$$= 1.39 \times 10^{-17} .$$

Here, the function $g(x)$ is the usual phase space factor in semi-leptonic meson decay, where constituent values of the final-state quark masses have been used.^[10] The QCD uncorrected $c \rightarrow u\gamma$ transition is seen to have an unobservably small branching fraction.

We next examine the impact of the QCD radiative corrections on the above branching ratios. We begin by reviewing the calculation for the $b \rightarrow s\gamma$ transition, which will serve as the foundation of our subsequent discussion of $c \rightarrow u\gamma$. The QCD corrections are calculated^[11, 12] via an operator product expansion based on the effective hamiltonian

$$H_{\text{eff}}^{|\Delta b|=1} = -\frac{4G_F}{\sqrt{2}} \lambda_t \sum_{k=1}^8 c_k(\mu) O_k(\mu) , \quad (9)$$

where the $\{O_k\}$ are a complete set of renormalized dimension-six operators involving light fields which govern the $b \rightarrow s$ transitions. They consist of two current-current operators $O_{1,2}$, four strong penguin operators O_{3-6} , and electro- and chromo-magnetic dipole operators O_7 and O_8 ,

$$\begin{aligned} O_1 &= (\bar{c}_\alpha \gamma_\mu P_L b_\beta) (\bar{s}_\beta \gamma^\mu P_L c_\alpha) , \\ O_2 &= (\bar{c}_\alpha \gamma_\mu P_L b_\alpha) (\bar{s}_\beta \gamma^\mu P_L c_\beta) , \\ O_3 &= (\bar{s}_\alpha \gamma_\mu P_L b_\alpha) \sum_q (\bar{q}_\beta \gamma^\mu P_L q_\beta) , \\ O_4 &= (\bar{s}_\alpha \gamma_\mu P_L b_\beta) \sum_q (\bar{q}_\beta \gamma^\mu P_L q_\alpha) , \\ O_5 &= (\bar{s}_\alpha \gamma_\mu P_L b_\alpha) \sum_q (\bar{q}_\beta \gamma^\mu P_R q_\beta) , \\ O_6 &= (\bar{s}_\alpha \gamma_\mu P_L b_\beta) \sum_q (\bar{q}_\beta \gamma^\mu P_R q_\alpha) , \\ O_7 &= \frac{e}{16\pi^2} m_b (\bar{s}_\alpha \sigma_{\mu\nu} P_R b_\alpha) F^{\mu\nu} , \\ O_8 &= \frac{g_s}{16\pi^2} m_b (\bar{s}_\alpha \sigma_{\mu\nu} T_{\alpha\beta}^a P_R b_\beta) G^{a\mu\nu} . \end{aligned} \quad (10)$$

The above effective hamiltonian is then evolved from the electroweak scale down to $\mu \sim m_b$ by the Renormalization Group Equations (RGE).

In the RG analysis, the Wilson coefficients are to be evaluated perturbatively at the W scale where the matching conditions are imposed and then

evolved down to the renormalization scale μ . The expressions for the $\{c_k\}$ at the W scale are

$$\begin{aligned} c_{1,3-6}(M_W) &= 0, & c_2(M_W) &= 1, \\ c_7(M_W) &= -\frac{1}{2}F_2(x_t), & c_8(M_W) &= -\frac{1}{2}D(x_t). \end{aligned} \quad (11)$$

with

$$D(x) = \frac{x^3 - 5x^2 - 2x}{4(x-1)^3} + \frac{3x^2 \ln x}{2(x-1)^4}. \quad (12)$$

The solution to the RGE at the leading logarithmic order is given by

$$c_k^{eff}(\mu) = U_{k\ell}^5(\mu, M_W) c_\ell(M_W), \quad (13)$$

where $U_{k\ell}^5$ denotes the evolution matrix in a five-flavor context and is determined by

$$U^5(m_1, m_2)_{kn} = O_{k\ell} \left[\eta^{\vec{a}_\ell} \right] O_{\ell n}^{-1}. \quad (14)$$

In the above we define $\eta \equiv \alpha_s(m_2)/\alpha_s(m_1)$ and $\vec{a}_\ell \equiv \gamma_{\ell\ell}^D/2\beta_0$ (*not* summed on ℓ), where $\beta_0 = 11 - 2n_f/3$ and $\gamma^D = O^{-1} \gamma^{(eff)T} O$ is the diagonalized form of the 8×8 anomalous dimension matrix. We use the scheme-independent form of the matrix γ^{eff} , which is given explicitly in Ref. [13] in terms of the number of $Q = +2/3$ and $Q = -1/3$ quarks present in the effective theory.

Scaling again to the semi-leptonic decay, the branching fraction is now given by

$$B_{b \rightarrow s\gamma} = \frac{6\alpha}{\pi} \cdot \left| \frac{V_{tb}V_{ts}^*}{V_{cb}} \right|^2 \cdot \frac{|c_7^{eff}(\mu)|^2}{g(m_c/m_b) + \frac{|V_{ub}|^2}{|V_{cb}|^2} g(m_u/m_b)} \cdot B_{B \rightarrow X\ell\nu}, \quad (15)$$

The numerical values of the separate contributions to $c_7^{eff}(\mu)$ are, with $m_t = 174$ GeV (for illustration purposes), $\mu = m_b = 4.87$ GeV, and $\alpha_s(M_Z) = 0.124$ as determined by LEP^[14],

$$\begin{aligned} c_7^{eff}(\mu) &= 0.670 c_7(M_W) + 0.091 c_8(M_W) - 0.172 c_2(M_W), \\ &= 0.670(-0.195) + 0.091(-0.097) - 0.172. \end{aligned} \quad (16)$$

Taking the overall CKM factor in the branching fraction to be unity, and $|V_{ub}|/|V_{cb}| = 0.08$, this procedure yields

$$B_{b \rightarrow s\gamma} = \left(2.92_{-0.59}^{+0.77} \right) \times 10^{-4}. \quad (17)$$

The central value corresponds to $\mu = m_b$, while the upper and lower errors represent the deviation due to assuming $\mu = m_b/2$ and $\mu = 2m_b$, respectively. We see that this value compares favorably to the recent CLEO measurement^[2] of the inclusive rate cited earlier in Eq. (2). When compared with the uncorrected result of Eq. (9), the QCD corrections are seen to increase the branching ratio by roughly a factor of 2.

We take this opportunity to reflect further on the size of the QCD corrections. Earlier estimates^[15] of these corrections found that the enhancements to the $b \rightarrow s\gamma$ branching fraction were more than an order of magnitude for $m_t < M_W$. This is because the effect of the QCD radiative correction to the weak vertex is to replace the GIM power suppression in Eq. (5) by a logarithmic suppression. We explicitly illustrate this effect in Fig. 2, where we show the dependence of the c_7 Wilson coefficient on the mass of a single internal quark using the calculational procedure described above. In the lower of the two curves, the dependence of c_7 determined at scale $\mu = m_W$ is displayed, while the upper curve corresponds to the evolved c_7 evaluated at $\mu = m_b$. We see that $c_7(\mu = m_b)$ is a reasonably flat function of the intermediate quark mass, and that the corrections are substantial for light internal quarks, with an increase of 3-4 orders of magnitude in the rate for $m_q = 5 - 10$ GeV. For the case of one heavy internal quark, *e.g.*, $b \rightarrow s\gamma$ with $m_t > M_W$, we see that the GIM mechanism no longer plays such a crucial role and the QCD enhancements are not as dramatic.



Figure 2. Dependence of c_7 on Intermediate-quark Mass

We now consider the case of radiative charm transitions. The $|\Delta c| = 1$ effective hamiltonian can be written as

$$H_{\text{eff}}^{|\Delta c|=1} = \frac{-4G_F}{\sqrt{2}} \lambda_b \sum_{k=1}^{10} c_k(\mu) O_k(\mu), \quad (18)$$

with $\lambda_i = V_{ci}^* V_{ui}$ as defined previously. The CKM structure of the operators differs dramatically from the $b \rightarrow s\gamma$ case. Here, both O_1 and O_2 have *two* contributions which have approximately equal CKM weighting since $\lambda_s \simeq \lambda_d$. We stress that extreme caution must be exercised in order to correctly incorporate these terms. To be precise we explicitly separate O_1 and O_2 into two operators according to their CKM structure,

$$\begin{aligned} O_{1a} &= (\bar{u}_\alpha \gamma_\mu P_L s_\beta) (\bar{s}_\beta \gamma^\mu P_L c_\alpha), & O_{1b} &= (\bar{u}_\alpha \gamma_\mu P_L d_\beta) (\bar{d}_\beta \gamma^\mu P_L c_\alpha), \\ O_{2a} &= (\bar{u}_\alpha \gamma_\mu P_L s_\alpha) (\bar{s}_\beta \gamma^\mu P_L c_\beta), & O_{2b} &= (\bar{u}_\alpha \gamma_\mu P_L d_\alpha) (\bar{d}_\beta \gamma^\mu P_L c_\beta), \end{aligned} \quad (19)$$

and write the remaining $|\Delta c| = 1$ operators in a form analogous to their $|\Delta b| = 1$ counterparts,

$$O_3 = (\bar{u}_\alpha \gamma_\mu P_L c_\alpha) \sum_q (\bar{q}_\beta \gamma^\mu P_L q_\beta),$$

$$\begin{aligned}
O_4 &= (\bar{u}_\alpha \gamma_\mu P_L c_\beta) \sum_q (\bar{q}_\beta \gamma^\mu P_L q_\alpha), \\
O_5 &= (\bar{u}_\alpha \gamma_\mu P_L c_\alpha) \sum_q (\bar{q}_\beta \gamma^\mu P_R q_\beta), \\
O_6 &= (\bar{u}_\alpha \gamma_\mu P_L c_\beta) \sum_q (\bar{q}_\beta \gamma^\mu P_R q_\alpha), \\
O_7 &= \frac{e}{16\pi^2} m_c (\bar{u}_\alpha \sigma_{\mu\nu} P_R c_\alpha) F^{\mu\nu}, \\
O_8 &= \frac{g_s}{16\pi^2} m_c (\bar{u}_\alpha \sigma_{\mu\nu} T_{\alpha\beta}^a P_R c_\beta) G^{a\mu\nu},
\end{aligned} \tag{20}$$

where the terms proportional to m_u in $O_{7,8}$ have again been neglected. Since the quantity $-\lambda_b$ has been factorized in Eq. (18) above, the values of the corresponding Wilson coefficients at the matching scale are now

$$\begin{aligned}
c_{1a}(M_W) &= 0, & c_{1b}(M_W) &= 0, \\
c_{2a}(M_W) &= -\lambda_s/\lambda_b, & c_{2b}(M_W) &= -\lambda_d/\lambda_b.
\end{aligned} \tag{21}$$

The values of the Wilson coefficients for $c_{3-6}(M_W)$ are the same as in Eq. (11), and the coefficients $c_{7,8}(M_W)$ are modified to

$$\begin{aligned}
c_7(M_W) &= -\frac{1}{2} \left[\frac{\lambda_s}{\lambda_b} F_2(x_s) + F_2(x_b) \right], \\
c_8(M_W) &= -\frac{1}{2} \left[\frac{\lambda_s}{\lambda_b} D(x_s) + D(x_b) \right],
\end{aligned} \tag{22}$$

with each containing intermediate s -quark and b -quark contributions. Due to the CKM dependence, $c_{7,8}(M_W)$ now contain both real and imaginary terms which in principle must be evolved separately. We note that the real parts of the x_s -dependent terms are numerically the same order of magnitude as the x_b terms. Now we evolve the effective theory down to the scale $\mu \sim m_c$. This takes place in two successive steps; first, we go from the electroweak scale down to m_b working in an effective 5 flavor theory, and then to $\mu < m_b$ in an effective 4 flavor theory. This procedure is similar to what is performed for the $|\Delta s| = 1$ kaon transitions^[16], where the effective theory is evolved to $\mu \sim 1$ GeV in 3 successive steps. We then have

$$\begin{aligned}
\mathcal{R}e c_k^{eff}(\mu) &= U_{k\ell}^4(\mu, m_b) U_{\ell n}^5(m_b, M_W) \mathcal{R}e c_n(M_W), \\
\mathcal{I}m c_k^{eff}(\mu) &= U_{k\ell}^4(\mu, m_b) U_{\ell n}^5(m_b, M_W) \mathcal{I}m c_n(M_W),
\end{aligned} \tag{23}$$

and

$$|c_7^{eff}(\mu)|^2 = |\mathcal{Re} c_7^{eff}(\mu)|^2 + |\mathcal{Im} c_7^{eff}(\mu)|^2. \quad (24)$$

The renormalization group evolution matrices U^4 and U^5 are determined as in Eq. (14) now using a 10×10 anomalous dimension matrix γ^{eff} . We take the anomalous dimensions of the split operators O_{1a-b} and O_{2a-b} to be exactly those for O_1 and O_2 , respectively, as the anomalous dimensions do not depend on the CKM structure of the operator. We use the form of γ^{eff} as given in Ref. [13], taking care to keep $n_f = 4$ and 5 as needed. The relative numerical values of the contributions to $c_7^{eff}(\mu)$ with $\mu = m_c = 1.5$ GeV are

$$\begin{aligned} c_7^{eff}(m_c) &\simeq \mathcal{Re} c_7^{eff}(m_c), \\ &= 0.458 c_7(M_W) + 0.125 c_8(M_W) - 0.312[c_{2a}(M_W) + c_{2b}(M_W)], \\ &= 0.458(-0.241 \times 10^{-6}) + 0.125(-0.139 \times 10^{-5}) - 0.312 \left(\frac{-\lambda_s - \lambda_d}{\lambda_b} \right), \\ &= 0.458(-0.241 \times 10^{-6}) + 0.125(-0.139 \times 10^{-5}) - 0.312, \end{aligned} \quad (25)$$

where the CKM unitarity condition $\lambda_s + \lambda_d = -\lambda_b$ has been used to simplify the final term. Incidentally, it should be stressed that the choice of $-\lambda_b$ as a prefactor in Eq. (18) was quite arbitrary, and we could have pulled out some other factor, say λ_s (or λ_d). This would have affected the Wilson coefficients at the matching scale, but the final result would have remained, as it must, unchanged.

We now compute the branching fraction. We evaluate α_s in the \overline{MS} scheme (using $\alpha_s(M_Z) = 0.124$ as before) and extend the range down to the charm scale using the Bernreuther matching conditions^[17] at the threshold $\mu = m_b = 4.87$ GeV. Note that we have also taken the CKM matrix elements to be real and have neglected any possible imaginary components. Given the small values of $c_{7,8}(M_W)$, this approximation is well justified. It is clear from the above that the $c_2(M_W)$ term completely dominates, due to the small contributions to $c_{7,8}(M_W)$ from the light internal quark masses. This is in stark contrast to $b \rightarrow s$ transitions (and likewise to $s \rightarrow d$), where the heavy internal t -quark forces the the magnetic dipole coefficients to be competitive with $c_2(M_W)$. This can be seen explicitly by comparing the above with

Eq. (16). The QCD-corrected branching fraction is then

$$\begin{aligned} \text{B}_{c \rightarrow u\gamma} &= \frac{6\alpha}{\pi} \cdot \left| \frac{V_{cb}^* V_{ub}}{V_{cs}} \right|^2 \cdot \frac{|c_7^{eff}(\mu)|^2}{g(m_s/m_c) + \frac{|V_{cd}|^2}{|V_{cs}|^2} g(m_d/m_c)} \cdot \text{B}_{D^+ \rightarrow X\ell^+\nu}, \\ &= (4.21 - 7.94) \times 10^{-12}, \end{aligned} \quad (26)$$

where the lower (upper) value in the numerical range corresponds to the scale $\mu = 2m_c(m_c)$. We see that the effects of the QCD corrections are quite dramatic in charm radiative decays, and that the rate is given almost entirely as a consequence of operator mixing. The stability of this result can be tested once the complete next-to-leading order corrections to the magnetic dipole transitions are known.

Finally, we wish to comment further on the CKM dependence of the $|\Delta b| = 1$ and $|\Delta c| = 1$ effective hamiltonians. We consider each case separately:

(i) $|\Delta b| = 1$ *transition*: Here, the the t -quark contribution is seen to dominate in every respect. Thus, for the dipole operators O_7 and O_8 , the u -quark and c -quark loops are omitted because they are numerically tiny (*e.g.*, see Table 2). Likewise, due to the smallness of the u -quark CKM factors, the approximation is made in the literature^[12] to omit any current-current operators containing u -quark fields. This explains why only the c -quark dependent operators $O_{1,2}$ appear in the $|\Delta b| = 1$ operator basis of Eq. (10). This assumption also explains another aspect of the analysis. Ordinarily one would expect $O_{1,2}$ to be accompanied by the CKM factor $-\lambda_c$, yet it is the prefactor λ_t which appears in the effective hamiltonian of Eq. (9). This is because the tiny value of λ_u has allowed one to write the CKM unitarity relation as $\lambda_c \simeq -\lambda_t$ and thus remove dependence upon λ_u .

(ii) $|\Delta c| = 1$ *transition*: In this case, the CKM dependence is more complicated since no single quark-loop is dominant. One must expand the operator basis as we did in Eq. (19). However, we wish to take note of a seemingly remarkable feature which occurs upon carrying out the RG analysis. The operators O_{2a} and O_{2b} turn out to have equal anomalous dimensions and thus c_{2a} and c_{2b} have the *same* numerical coefficient in Eq. (25). The most elegant way to understand this result is to exploit the U -spin symmetry present in the system of operators $O_{1a,1b}$ and $O_{2a,2b}$. Thus, suppose instead of proceeding as we did, we replaced the operators O_{2a} and O_{2b} of Eq. (19)

with the equivalent set O'_{2a} and O'_{2b} , where

$$\begin{aligned}
O_{2a} \rightarrow O'_{2a} &\equiv \frac{1}{2}(O_{2a} + O_{2b}) \\
&= \frac{1}{2} \left[(\bar{u}_\alpha \gamma_\mu P_L s_\alpha) (\bar{s}_\beta \gamma^\mu P_L c_\beta) + (\bar{u}_\alpha \gamma_\mu P_L d_\alpha) (\bar{d}_\beta \gamma^\mu P_L c_\beta) \right], \\
O_{2b} \rightarrow O'_{2b} &\equiv \frac{1}{2}(O_{2a} - O_{2b}) \\
&= \frac{1}{2} \left[(\bar{u}_\alpha \gamma_\mu P_L s_\alpha) (\bar{s}_\beta \gamma^\mu P_L c_\beta) - (\bar{u}_\alpha \gamma_\mu P_L d_\alpha) (\bar{d}_\beta \gamma^\mu P_L c_\beta) \right],
\end{aligned} \tag{27}$$

along with a corresponding replacement of coefficients,

$$c_{2a} \rightarrow c'_{2a} \quad \text{and} \quad c_{2b} \rightarrow c'_{2b} . \tag{28}$$

The matching conditions for the modified coefficients would then have become

$$c'_{2a}(M_W) = \frac{\lambda_s + \lambda_d}{-\lambda_b} = 1 \quad \text{and} \quad c'_{2b}(M_W) = \frac{\lambda_s - \lambda_d}{-\lambda_b} , \tag{29}$$

with analogous replacements made also for O_{1a} and O_{1b} . Since the mixing of O_{2a} and O_{2b} with O_7 has no dependence on the mass of the internal s and d quarks, the operator O'_{2b} does not contribute to the process $c \rightarrow u + \gamma$ due to cancellation between the s -quark and d -quark contributions. This cancellation is in fact just the manifestation of an underlying U -spin symmetry. That is, in the limit of neglecting quark mass, O'_{2b} carries U -spin 1 and thus cannot couple to a photon. This decoupling occurs via the very s -quark and d -quark cancellation under discussion. As a consequence, the other operator O'_{2a} must have the the same anomalous dimension as O_{2a} under RG flow, and we obtain the result cited above.

As a corollary, it is clear that in the $|\Delta b| = 1$ transition, the approximation made of omitting the u -quark current-current operators is quite unnecessary. One could just as easily deal with an expanded operator basis containing u -quark fields analogous to that of Eq. (19) or by invoking an $SU(4)$ version of u -quark/ c -quark U -spin symmetry and proceeding as above.

3 Long Distance Pole Contributions

As seen in the previous section, the short distance contributions to charm radiative decays give very small branching ratios, even when the large QCD

enhancement is taken into account. There will, however, be additional contributions that appear as exclusive modes for which the momentum scale of the intermediate quarks is a strong interaction scale and not the short distance scale M_W . This forces us to view the intermediate states as hadrons rather than quarks. These long distance contributions can be partitioned into two basic classes. The first corresponds, at the quark level, to annihilation diagrams $c\bar{q}_1 \rightarrow q_2\bar{q}_3$ where a photon line is attached to any of the four quark lines. In terms of hadronic degrees of freedom, these give rise to the set of contributions which include the *pole diagrams*. The second type of contribution corresponds to the underlying quark processes $c \rightarrow q_1\bar{q}_2q$, followed by $\bar{q}_2q \rightarrow \gamma$. At the hadronic level, this is the so-called *vector meson dominance* mechanism. We shall discuss the pole amplitudes in this section, leaving consideration of the VMD mechanism for Section 4.

The pole amplitudes are but a subset of an entire class of long-distance contributions, including the two-particle intermediate states and proceeding to all higher n -particle intermediate states. However, of these the most phenomenologically accessible are the single-particle or pole terms. The relevant diagrams, appearing in Figs. 3(a,b), are seen to fall into either of two basic classes. We shall refer to transitions as type I if weak-mixing occurs before photon emission, *i.e.* if the incoming D meson experiences weak-mixing, and as type II if photon emission occurs before weak-mixing, *i.e.* if the final state meson is created via weak-mixing. In principle, the intermediate states occurring in the type I and type II amplitudes consist respectively of all possible virtual spin-zero and spin-one particles. We shall find it practicable, however, to take into account only the lightest such virtual particles.



Figure 3. Pole Contributions

In analyzing long range effects for flavor-changing D decays, we shall

employ the effective weak hamiltonian of Bauer, Stech and Wirbel^[19] (BSW),

$$\mathcal{H}_w = -\frac{G_F}{\sqrt{2}} [: a_1(\bar{u}d')(\bar{s}'c) + a_2(\bar{s}'d')(\bar{u}c) :] \quad , \quad (30)$$

where the colons denote normal-ordering and d', s' are the CKM-mixed fields

$$\begin{aligned} d' &= V_{ud} d + V_{us} s \quad , \\ s' &= V_{cs} s + V_{cd} d \quad . \end{aligned} \quad (31)$$

We shall work in the 2×2 basis of quark flavors,

$$\mathbf{V} = \begin{pmatrix} V_{ud} & V_{us} \\ V_{cd} & V_{cs} \end{pmatrix} \simeq \begin{pmatrix} 0.975 & 0.222 \\ -0.222 & 0.975 \end{pmatrix} \quad . \quad (32)$$

Specific forms for the Cabibbo-favored and Cabibbo-suppressed hamiltonians will be given shortly. The quark fields occur in left-handed combinations, denoted by

$$(\bar{q}_1 q_2) \equiv \bar{q}_1 \gamma_\mu (1 + \gamma_5) q_2 \quad , \quad (33)$$

and a_1, a_2 are free parameters whose values will generally depend on the mass scale being probed. Here, they are determined by fitting to $D \rightarrow \bar{K}\pi$ data^[20],

$$a_1(m_c^2) = 1.2 \pm 0.1 \quad , \quad a_2(m_c^2) = -0.5 \pm 0.1 \quad . \quad (34)$$

Pole Amplitudes of Type I

Among the possible exclusive D decays, the most promising for experimental detection occur in the class of vector meson–photon ($V\gamma$) final states,

$$D(\mathbf{p}) \rightarrow V(\mathbf{k}, \lambda) + \gamma(\mathbf{q}, \sigma) \quad . \quad (35)$$

For these, the transition amplitude has the gauge invariant form

$$\mathcal{M}_{D \rightarrow V\gamma} = \epsilon_\mu^\dagger(k, \lambda) \epsilon_\nu^\dagger(q, \sigma) \left[\mathcal{A}^{\text{pv}} (p^\mu p^\nu - g^{\mu\nu} q \cdot p) + i \mathcal{A}^{\text{pc}} \epsilon^{\mu\nu\alpha\beta} k_\alpha p_\beta \right] \quad . \quad (36)$$

The parity-violating and parity-conserving amplitudes are denoted by \mathcal{A}^{pv} and \mathcal{A}^{pc} respectively, and each carries the dimension of inverse energy. Both

amplitudes are generally required because the weak interaction does not respect parity invariance. The $D \rightarrow V\gamma$ decay rate is given by

$$\Gamma_{D \rightarrow V\gamma} = \frac{|\mathbf{q}|^3}{4\pi} (|\mathcal{A}^{\text{pv}}|^2 + |\mathcal{A}^{\text{pc}}|^2) \ , \quad (37)$$

where \mathbf{q} is the decay momentum in the D rest frame,

$$|\mathbf{q}| = \frac{m_D^2 - m_V^2}{2m_D} \ . \quad (38)$$

Which particular combination of the parity-conserving and parity-violating amplitudes contributes to the decay process will depend upon the weak-mixing amplitude. In principle, a charm meson can mix with a sequence of either scalar $\{S_n\}$ or pseudoscalar $\{P_n\}$ mesons. Although some work on scalar-mixing has been done,^[18] the outcome is rather model-dependent because detailed experimental and theoretical understanding about scalar states is lacking. In this paper, we shall therefore consider only the weak-mixing of charm mesons with light pseudoscalar mesons and thus work with only parity-conserving (PC) pole amplitudes.

It is appropriate at this point to comment on the notation to be employed from this point on in both Section 3 and Section 4. We shall denote f_P as the decay constant of pseudoscalar meson P and define $h_{V\gamma P}$ as the coupling constant for the EM interaction vertex of the photon γ with the mesons V, P . Also, the decay constant of vector meson V is given in terms of the V -to-vacuum matrix element of the vector current,

$$\langle 0|V_\mu^a|V^b(\mathbf{q}, \lambda)\rangle = \delta^{ab} \frac{m_V^2}{f_V} \epsilon_\mu^*(\mathbf{q}, \lambda) \equiv \delta^{ab} g_V \epsilon_\mu^*(\mathbf{q}, \lambda) \ . \quad (39)$$

Note that we define two equivalent parameterizations, g_V (with units of GeV^2) and f_V (dimensionless), for the vector decay constant. We have found that employing g_V in the discussion of pole amplitudes alleviates notational confusion which would otherwise occur between the vector and pseudoscalar decay constants f_V and f_P . However, it is traditional to use f_V in discussing VMD amplitudes, and we do so in Section 4. The constants $\{f_V\}$ are obtained from $\Gamma_{V \rightarrow l+l^-}$ data and have recently been compiled in Table 1 of Ref. [3].

Now, a pseudoscalar state P which is created by weak mixing will propagate virtually until it eventually decays into the final state. This latter

transition is electromagnetic and hence parity-conserving. It has the amplitude

$$\mathcal{M}_{V\gamma P} = h_{V\gamma P} \epsilon_\mu^\dagger(k, \lambda) \epsilon_\nu^\dagger(q, \sigma) \epsilon^{\mu\nu\alpha\beta} k_\alpha p_\beta . \quad (40)$$

The absolute value of the coupling constant $h_{V\gamma P}$ can be inferred phenomenologically by using

$$|h_{V\gamma P}|^2 = \begin{cases} 12\pi\Gamma_{V\rightarrow P\gamma}/|\mathbf{q}|^3 & (M_V > M_P) \\ 4\pi\Gamma_{P\rightarrow V\gamma}/|\mathbf{q}|^3 & (M_P > M_V) . \end{cases} \quad (41)$$

The general type I decay amplitude \mathcal{A}_I for $D \rightarrow V\gamma$ is then given by

$$\mathcal{A}_I^{\text{pc}}(D \rightarrow V\gamma) = \sum_n h_{V\gamma P_n} \cdot \frac{1}{m_D^2 - m_{P_n}^2} \cdot \langle P_n | \mathcal{H}_w^{(\text{eff})} | D \rangle . \quad (42)$$

With Fig. 3(a) as a guide, the notation should be self-evident.

Predictions for $D \rightarrow V\gamma$ decay amplitudes will be obtained below in terms of both type I and type II pole amplitudes, and in the next section we shall do the same by using VMD amplitudes. We can, however, accomplish somewhat more. In principle, the discussion for $V\gamma$ final states extends to a larger set of meson-photon final states $M\gamma$, where the only restriction on meson M is that it have spin greater than zero. For each different type of $M\gamma$ final state, there will be a gauge invariant D -decay amplitude like Eq. (36) and an $M\gamma P$ interaction vertex like Eq. (40). However, the generic form of Eq. (42) continues to hold, except that $h_{V\gamma P_n}$ is replaced by $h_{M\gamma P_n}$. Of course, to have predictive power requires knowledge of the $h_{M\gamma P_n}$ coupling constant. Fortunately, much has been learned about radiative decays in light meson systems over the years. In particular, there are varying amounts of experimental evidence for 17 such transitions in the listing of Ref. [6]. Of these, 10 involve $1^- \rightarrow 0^-$ mesonic transitions, 3 involve $2^+ \rightarrow 0^-$, 2 involve $1^+ \rightarrow 0^-$ and 2 involve $0^- \rightarrow 1^-$. This information allows us to extend the analysis of type I amplitudes from just $V\gamma$ final states to include both $A\gamma$ and $T\gamma$ configurations as well, where ‘ A ’ and ‘ T ’ stand for axialvector and tensor mesons respectively. The $A\gamma$ final states are very analogous to the $V\gamma$ decays in that the coupling constant $h_{A\gamma P_n}$ is found via Eq. (41) and the $D \rightarrow A\gamma$ decay amplitude has the same form as Eq. (37). For the $T\gamma$ final states, one uses instead

$$|h_{T\gamma P}|^2 = \frac{40\pi\Gamma_{T\rightarrow P\gamma}}{|\mathbf{q}|^5} \quad (43)$$

as well as

$$\Gamma_{D \rightarrow T\gamma} = \frac{|\mathbf{q}|^5}{4\pi} |\mathcal{A}_I^{\text{pc}}|^2 . \quad (44)$$

To summarize, we shall include in our study of type I amplitudes certain $D \rightarrow A\gamma$ and $D \rightarrow T\gamma$ transitions. For the type II or VMD amplitudes, however, we shall limit our calculations to just the $V\gamma$ final states.

Cabibbo-favored (CF) transitions:

In this case, the BSW hamiltonian becomes

$$\mathcal{H}_w^{(\text{CF})} = -V_{ud}V_{cs}^* \frac{G_F}{\sqrt{2}} [: a_1(\bar{u}d)(\bar{s}c) + a_2(\bar{s}d)(\bar{u}c) :] . \quad (45)$$

The calculation of weak-mixing matrix elements of D 's with the light pseudoscalar mesons is straightforward and results are tabulated in Table 4. The fact that these mixing amplitudes are evaluated in vacuum saturation makes the forms in Table 4 easy to interpret. Thus, for example, in Cabibbo-favored D_s^+ decay, it is the term in the BSW hamiltonian with coefficient a_1 which contributes, and as such, the weak-mixing matrix element is naturally proportional to the decay constants f_π and $f_{D_s^+}$.

Table 4 Cabibbo-favored Mixing Amplitudes

Mixing	Matrix Element
$D_s^+ \rightarrow \pi^+$	$a_1 V_{ud} V_{cs}^* f_\pi f_{D_s^+} m_{D_s^+}^2 G_F / \sqrt{2}$
$D^0 \rightarrow \bar{K}^0$	$a_2 V_{ud} V_{cs}^* f_K f_D m_{D^0}^2 G_F / \sqrt{2}$
$D^+ \rightarrow \pi^+$	0

For the decay constants of the light mesons we use

$$f_\pi = 131 \text{ MeV} \quad \text{and} \quad f_K = 161 \text{ MeV} . \quad (46)$$

The present situation for the decay constants f_D and f_{D_s} of the charm mesons is somewhat problematic. Experiment provides the upper limit for f_D ,

$$f_D < 290 \text{ MeV} , \quad (47)$$

as obtained from the branching ratio determination $Br_{D^+ \rightarrow \mu^+ \nu_\mu} < 7.2 \times 10^{-4}$ at 90% confidence-level^[21]. Thus only theoretical estimates exist for f_D . These occur in three categories, lattice theoretic^[22], QCD sum rule^[23] and quark model fits to color-hyperfine mass splittings^[24]. Estimates fall in the range $185 < f_D(\text{MeV}) < 262$. We shall adopt the value

$$f_D^{\text{latt.}} \simeq 216 \text{ MeV} \quad , \quad (48)$$

which is an average over the lattice estimates^[25] and falls between the other two types of determinations.

Recently, the following experimental results (in units of MeV) for f_{D_s} were announced by CLEO^[26], WA75^[27] and BES^[28],

$$f_{D_s} = \begin{cases} 344 \pm 37 \pm 67 & (\text{CLEO}) \\ 232 \pm 45 \pm 52 & (\text{WA75}) \\ 434_{-133}^{+153} \pm_{-33}^{+35} & (\text{BES}) \quad , \end{cases} \quad (49)$$

where the CLEO value is inferred from the ratio $\Gamma_{D_s^+ \rightarrow \mu^+ \nu_\mu} / \Gamma_{D_s^+ \rightarrow \phi \pi^+}$ along with the branching ratio $B_{D_s^+ \rightarrow \phi \pi^+}$. In our numerical analysis, we shall use the following weighted average of the above decay constants,

$$f_{D_s}^{\text{expt.}} = 299 \text{ MeV} \quad . \quad (50)$$

For the sake of comparison, we note that this value is somewhat larger than the central value of a weighted average taken from a compilation of existing lattice estimates,^[25]

$$f_{D_s}^{\text{latt.}} = 242 \text{ MeV} \quad . \quad (51)$$

The only other ingredients needed are the radiative coupling constants $h_{M\gamma P}$, which were defined earlier. Putting together all the necessary ingredients and ranging over the set of final state mesons $M = \rho(770)$, $K^*(892)$, $b_1(1235)$, $a_1(1270)$, $a_2(1320)$ and $K_2^*(1430)$ yields the magnitudes of type I pole-model amplitudes (in units of GeV^{-1}) given in Table 5.

Table 5 Type I Cabibbo-favored Decay

Mode	$ \mathcal{A}_I^{\text{pc}} \text{ (GeV}^{-1}\text{)}$
$D_s^+ \rightarrow \rho^+ \gamma$	8.2×10^{-8}
$D_s^+ \rightarrow b_1^+(1230) \gamma$	7.2×10^{-8}
$D_s^+ \rightarrow a_1^+(1270) \gamma$	1.2×10^{-7}
$D_s^+ \rightarrow a_2^+(1320) \gamma$	2.1×10^{-7}
$D^0 \rightarrow \bar{K}^{*0} \gamma$	5.6×10^{-8}

These values should be considered as upper bounds for the following reason. We have considered the lightest possible intermediate states, pions and kaons, because only for these particles is there sufficient data for determining coupling constants. However, the pion and kaon intermediate states propagate far off-shell. Instead of having a squared momentum near the mass-shell value $q^2 = m_\pi^2$, the virtual pion must carry $q^2 = m_{D_s}^2 \gg m_\pi^2$ and similarly for the kaon. This effect could well suppress the transition amplitude.

In principle, one is to sum over all pion-like and kaon-like intermediate states. Other possible contributions should be heavier and thus less affected by this suppression effect. For pion-like intermediate states, the next state in order of increasing mass would be $\pi(1300)$ and beyond that the unconfirmed state $\pi(1770)$. Although there is not sufficient data to make a numerical estimate of their effect, we can anticipate for such states that

- (i) the propagator contribution will indeed be larger,
- (ii) the weak-mixing between a ground state D meson and a radially excited meson P_n will be wave-function suppressed,
- (iii) the radiative coupling constant $h_{M\gamma P_n}$ might well be relatively smaller due to phase space competition with other decay modes of the massive meson P_n .

We would expect the net result of these effects to decrease the overall contribution from the excited states.

Cabibbo-suppressed (CS) transitions:

The weak-mixing now proceeds according to the weak hamiltonian

$$\begin{aligned} \mathcal{H}_w^{(\text{CS})} = & -\frac{G_F}{\sqrt{2}} \left[: a_1 \left(V_{ud}V_{cd}^*(\bar{u}d)(\bar{d}c) + V_{us}V_{cs}^*(\bar{u}s)(\bar{s}c) \right) \right. \\ & \left. + a_2 \left(V_{us}V_{cs}^*(\bar{s}s)(\bar{u}c) + V_{ud}V_{cd}^*(\bar{d}d)(\bar{u}c) \right) : \right] , \end{aligned} \quad (52)$$

The action of the $(\bar{d}d)$ and $(\bar{s}s)$ operators on the vacuum when expressed in terms of the pseudoscalar meson states becomes

$$\begin{aligned} (\bar{d}d) &= -0.7071\pi^0 + 0.58\eta + 0.40\eta' \\ (\bar{s}s) &= -0.57\eta + 0.82\eta' , \end{aligned} \quad (53)$$

where an $\eta - \eta'$ mixing angle $\theta_P = -20^\circ$ is adopted.^[29] In addition, we take^[29]

$$f_\eta \simeq f_{\eta'} \simeq f_\pi . \quad (54)$$

The mixing amplitudes which are relevant for Cabibbo-suppressed decay appear in Table 6. Observe that we have simplified the notation for D^0 transitions by expressing $V_{ud}V_{cd}^*$ in terms of $V_{us}V_{cs}^*$.

Table 6 Cabibbo-suppressed Mixing Amplitudes

Mixing	Matrix Element
$D^+ \rightarrow \pi^+$	$a_1 V_{ud} V_{cd}^* f_\pi f_{D^+} m_{D^+}^2 G_F / \sqrt{2}$
$D_s^+ \rightarrow K^+$	$a_1 V_{us} V_{cs}^* f_K f_{D_s^+} m_{D_s^+}^2 G_F / \sqrt{2}$
$D^0 \rightarrow \pi^0$	$0.7071 a_2 V_{us} V_{cs}^* f_{D^0} f_\pi m_{D^0}^2 G_F / 2$
$D^0 \rightarrow \eta$	$-1.15 a_2 V_{us} V_{cs}^* f_{D^0} f_\eta m_{D^0}^2 G_F / 2$
$D^0 \rightarrow \eta'$	$0.42 a_2 V_{us} V_{cs}^* f_{D^0} f_{\eta'} m_{D^0}^2 G_F / 2$

The analysis for Cabibbo-suppressed decays proceeds analogous to that for Cabibbo-favored decays, with one significant complication. For each of the Cabibbo-favored transitions, only one amplitude contributes. For D^0 decay, however, all the Cabibbo-suppressed pole amplitudes contain a sum over π^0 , η and η' intermediate states. It is important to get the relative phases of the interfering amplitudes correct. We have therefore performed an analysis of the nine $V^0 \rightarrow P^0 \gamma$ couplings in light of the most recent data, where $V^0 = \rho^0, \omega^0, \phi^0$ and $P^0 = \pi^0, \eta$ and η' .^[30] The magnitudes of the Cabibbo-suppressed amplitudes are displayed in Table 7.

Table 7 Type I Cabibbo-suppressed Decay

Mode	$ \mathcal{A}_I^{\text{pc}} \text{ (GeV}^{-1}\text{)}$
$D^+ \rightarrow \rho^+ \gamma$	1.3×10^{-8}
$D^+ \rightarrow b_1^+(1230) \gamma$	1.2×10^{-8}
$D^+ \rightarrow a_1^+(1270) \gamma$	4.9×10^{-9}
$D^+ \rightarrow a_2^+(1320) \gamma$	3.4×10^{-8}
$D_s^+ \rightarrow K^{*+} \gamma$	2.8×10^{-8}
$D_s^+ \rightarrow K_2^{*+}(1430) \gamma$	6.0×10^{-8}
$D^0 \rightarrow \rho^0 \gamma$	4.8×10^{-9}
$D^0 \rightarrow \omega^0 \gamma$	6.1×10^{-9}
$D^0 \rightarrow \phi^0 \gamma$	7.4×10^{-9}

Pole Amplitudes of Type II

Analogous to the type I $D \rightarrow V\gamma$ decay amplitude of Eq. (42) we have

$$\mathcal{A}_{II}^{\text{pc}}(D \rightarrow V\gamma) = \sum_n \langle V | \mathcal{H}_w^{(\text{eff})} | D_n^* \rangle \cdot \frac{1}{m_D^2 - m_{D_n^*}^2} \cdot h_{D_n^* \gamma D} \quad (55)$$

for the corresponding type II transition. From the viewpoint of phenomenology, the type II transitions are more problematic than are those of type I because less experimental input is available. Thus, we shall need to rely a bit more heavily on theoretical predictions.

The first difficulty is that the couplings $h_{D^{*0}\gamma D^0}$, $h_{D^{*+}\gamma D^+}$, and $h_{D_s^{*+}\gamma D_s^+}$ have not yet been experimentally measured. This is because, although the relevant photonic branching ratios have been measured, only upper bounds exist for the full widths of the associated spin-one excited states, D^{*0} , D^{*+} and D_s^{*+} ,

$$\begin{aligned} \Gamma_{D^{*0}} < 2100 \text{ keV} &\implies \Gamma_{D^{*0} \rightarrow D^0 \gamma} < 764 \text{ keV} \\ \Gamma_{D^{*+}} < 131 \text{ keV} &\implies \Gamma_{D^{*+} \rightarrow D^+ \gamma} < 1.44 \text{ keV} \\ \Gamma_{D_s^{*+}} < 4500 \text{ keV} &\implies \Gamma_{D_s^{*+} \rightarrow D_s^+ \gamma} < 4500 \text{ keV} . \end{aligned} \quad (56)$$

Fortunately, predictions for the $\Gamma_{D^{*0} \rightarrow D^0 \gamma}$, $\Gamma_{D^{*+} \rightarrow D^+ \gamma}$ and $\Gamma_{D_s^{*+} \rightarrow D_s^+ \gamma}$ transitions have appeared in the literature recently.[31, 32, 33, 34] There is some spread in predictions, and so we choose the representative values,

$$\Gamma_{D^{*0} \rightarrow D^0 \gamma} = 20 \text{ keV} , \quad \Gamma_{D^{*+} \rightarrow D^+ \gamma} = 0.5 \text{ keV} , \quad \Gamma_{D_s^{*+} \rightarrow D_s^+ \gamma} = 0.3 \text{ keV} , \quad (57)$$

which implies

$$\begin{aligned} h_{D^{*0}\gamma D^0} &= 0.542 \text{ GeV}^{-1} , \\ h_{D^{*+}\gamma D^+} &= -0.087 \text{ GeV}^{-1} , \\ h_{D_s^{*+}\gamma D_s^+} &= -0.066 \text{ GeV}^{-1} , \end{aligned} \quad (58)$$

where we have adopted the phases implied by the quark model. A rough check on whether the above values are reasonable is afforded by the nonrelativistic

quark model, in which

$$\begin{aligned}
h_{D^{*0}\gamma D^0} &= 2e \left[\frac{1}{M_c} + \frac{1}{M_u} \right] , \\
h_{D^{*+}\gamma D^+} &= e \left[\frac{2}{M_c} - \frac{1}{M_d} \right] , \\
h_{D_s^{*+}\gamma D_s^+} &= e \left[\frac{2}{M_c} - \frac{1}{M_s} \right] ,
\end{aligned} \tag{59}$$

where the $\{M_k\}$ are constituent quark masses, distinct from the current masses $\{m_k\}$ of Section 2. If we take $M_c \simeq 1.64$ GeV, as implied by a fit to D and D^* masses, then the relations in Eqs. (57-59) yield $M_u \simeq M_d = 0.48$ GeV and $M_s \simeq 0.53$ GeV.

The other of the difficulties concerns the weak-mixing matrix elements. For type II transition amplitudes, the mixing occurs between charm and light vector mesons, as in

$$\langle \rho^+ | \mathcal{H}_w^{(\text{eff})} | D_s^{*+} \rangle \simeq a_1 V_{ud} V_{cs} g_{\rho^+} g_{D_s^{*+}} G_F / \sqrt{2} . \tag{60}$$

In the above, the g_V are the vector meson decay constants defined in Eq. (39) and whose determination we shall discuss shortly. As with the type I amplitudes, we have employed vacuum saturation. To determine the action of the $(\bar{d}d)$ and $(\bar{s}s)$ operators upon the vacuum we employ the ideally-mixed vector meson states, so that

$$(\bar{d}d) = \frac{\omega - \rho^0}{\sqrt{2}} \quad \text{and} \quad (\bar{s}s) = \phi . \tag{61}$$

For the light 1^- mesons, the collection $\{g_V\}$ of vector decay constants can be determined by referring to the vacuum-to-meson matrix elements of J_{em}^μ given in Table 1 of Ref. [3]. Together with isospin and $SU(3)$ relations along with quark model insights, these generate all the needed values, *e.g.*

$$g_{\rho^+} \simeq 0.17 \text{ GeV}^2 , \quad g_{K^*} \simeq \frac{m_{K^*}^2}{m_\rho^2} g_{\rho^+} \simeq 0.22 \text{ GeV}^2 , \quad \dots . \tag{62}$$

To estimate the D_s^{*+} and D^{*0} decay constants, we invoke the heavy-quark-symmetry relations,

$$\begin{aligned}
g_{D_s^*} &= m_{D_s} f_{D_s} \simeq 0.588 \text{ GeV}^2 , \\
g_{D^*} &= m_D f_D \simeq 0.403 \text{ GeV}^2 .
\end{aligned} \tag{63}$$

The magnitudes of the type II amplitudes thus calculated are given in Table 8.

Table 8 Type II Decays

Mode	$ \mathcal{A}_{II}^{\text{pc}} $ (GeV $^{-1}$)
$D_s^+ \rightarrow \rho^+ \gamma$	1.9×10^{-8}
$D^0 \rightarrow \bar{K}^{*0} \gamma$	5.9×10^{-8}
$D^+ \rightarrow \rho^+ \gamma$	3.6×10^{-9}
$D_s^+ \rightarrow K^{*+} \gamma$	5.1×10^{-9}
$D^0 \rightarrow \rho^0 \gamma$	4.7×10^{-9}
$D^0 \rightarrow \omega^0 \gamma$	6.9×10^{-9}
$D^0 \rightarrow \phi^0 \gamma$	1.6×10^{-8}

D^* excitations with spins not equal to one will not contribute to type II amplitudes if we adhere strictly to the hamiltonian of Eq. (30)^[3] and continue to work within the vacuum saturation framework. The reason is that mesons with $J > 1$ cannot have a nonzero matrix element with the vacuum via the current $\bar{q}\gamma_\mu(1 + \gamma_5)c$. The possibility of an intermediate charm meson with $J = 0$ is disallowed since it could only mix with a final-state $J = 0$ particle and the decay of a spinless particle to another spinless particle plus a photon is forbidden.

Although we have considered just final state vector mesons in Table 8, it should be obvious that in principle the spin-one intermediate D^* states can also mix weakly with axialvector final state mesons. Unfortunately, one knows less about the decay constants of axialvector mesons than one does of the vector mesons.

4 Long Distance VMD Contributions

The VMD contribution to charm meson radiative decay is depicted in Fig. 4, where a D meson is seen to (i) decay weakly into a final state of a vector meson V and a meson M of nonzero spin, followed by (ii) an electromagnetic VMD conversion of V into a photon. Roughly speaking, in the VMD approach the $D \rightarrow M\gamma$ amplitude is obtained by multiplying the $D \rightarrow MV$ amplitude by the factor e/f_V where e is the electric charge and f_V is the dimensionless

version of the vector meson decay constant defined in Eq. (39). It is important to keep in mind that in the VMD process $D \rightarrow MV$, the vector meson V is off-shell. Thus, to obtain the VMD amplitude for $D \rightarrow M\gamma$ will require an extrapolation from $p_V^2 = m_V^2$ to $p_V^2 = 0$ for both the $V \rightarrow \gamma$ vertex and the $D \rightarrow MV$ transition. For our considerations, the main intermediate states will involve virtual rho and phi mesons. We shall employ the observation made in Ref. [35] that the rho-gamma vertex seems to be unaffected by the extrapolation whereas the phi-gamma vertex is reduced by a factor of $\eta_\phi \simeq \sqrt{2}$. In the following, we will consider a number of examples for the case $M = V$, and so we shall be working with VMD chains which begin with the process $D \rightarrow VV$. Since the VV final states have $L = 0, 1, 2$ as allowed orbital angular momentum values, the VMD amplitude will in general have a parity-conserving part $\mathcal{A}_{\text{VMD}}^{\text{pc}}$ corresponding to the VV P -wave and a parity-violating part $\mathcal{A}_{\text{VMD}}^{\text{pv}}$ corresponding to the VV S -wave and/or D -wave.



Figure 4. VMD Contribution

In practice, there are two means for determining the $D \rightarrow MV$ part of a VMD amplitude for $D \rightarrow M\gamma$:

1. One can input $D \rightarrow MV$ experimental data directly in order to phenomenologically determine the $D \rightarrow MV$ amplitude. In this approach, it is crucial to maintain gauge invariance. A careful discussion of how to construct a gauge invariant amplitude was recently given in Ref. [3] (which considered this type of empirical VMD contribution to $B \rightarrow K^*\gamma$), so we need not detail this procedure here. Since the database for $D \rightarrow MV$ transitions is unfortunately small, the ability to generate VMD amplitudes using this phenomenological method is limited.

2. One can employ some theoretical description to model the $D \rightarrow MV$ amplitude. Since the models currently available do not always reliably reproduce branching ratios and polarizations of final-state vector mesons in decays of heavy mesons,^[36] this method is also not beyond criticism. For definiteness, we shall continue to employ the BSW model^[19] introduced in Section 3.^[37] Within this approach, the squared VMD amplitude for the important case where M is a vector meson becomes

$$|\mathcal{A}_{\text{VMD}}|^2 = \frac{G_F^2 |V_{cq}^* V_{qu}|^2}{2m_D^2 \mathbf{k}^2} a_i^2(m_c^2) f_X^2 I \times \left[(m_D + m_Y)^2 A_1^2(q_0^2) + \frac{4\mathbf{k}^2 m_D^2 V^2(q_0^2)}{(m_D + m_Y)^2} \right] \times \left(\frac{4\pi\alpha}{f_V^2} \right), \quad (64)$$

where $|\mathbf{k}|$ is the photon spatial momentum, q represents either of the d or s light quarks, and I is a process-dependent isospin coefficient. The BSW coefficients $a_1(m_c^2)$ and $a_2(m_c^2)$ which correspond to the color-favored and color-suppressed operators are given in Eq. (34). The remaining notation is explained by noting that in the factorization approximation for $D \rightarrow MV$, one of the final state particles, which we call X (either M or V), couples directly to the vacuum and the other, which we call Y (either V or M), appears in the D -to- Y matrix element of the charged weak current J_{ch}^μ . Thus the quantity f_X is the decay constant of X , and $A_1(q^2)$ and $V(q^2)$ are the semileptonic form factors defined by

$$\begin{aligned} \langle Y(p_Y) | J_{\text{ch}}^\mu | D(P) \rangle = & \frac{2V(q^2)}{m_D + m_Y} \epsilon^{\mu\nu\rho\sigma} \epsilon_\nu^* P_\rho p_{Y\sigma} + 2m_Y i A_0(q^2) \frac{\epsilon^* \cdot q}{q^2} q^\mu \\ & + i \left[(m_D + m_Y) A_1(q^2) \epsilon^{*\mu} - \frac{\epsilon^* \cdot q A_2(q^2)}{m_D + m_Y} (P + p_Y)^\mu \right. \\ & \left. - 2m_Y A_3(q^2) \frac{\epsilon^* \cdot q}{q^2} q^\mu \right]. \end{aligned} \quad (65)$$

In the VMD amplitude, the form factors are to be evaluated at $q_0^2 = 0$ if $X = V$ and at $q_0^2 = m_M^2$ if $X = M$. Throughout, we shall make use of the form factors as measured^[38] in $D \rightarrow K^* l \nu$ and also employ

$SU(3)$ relations as needed. This should provide a good estimate of the form factors appearing in the D -to- ρ and D -to- ϕ matrix elements. Whenever the form factors are to be evaluated at momentum transfers other than at $q^2 = 0$, we shall use a monopole form to extrapolate from $q^2 = 0$. This amounts simply to dividing the form factors at $q^2 = 0$ by the quantity $1 - q^2/m_{\text{pole}}^2$.

In the following, we shall give VMD predictions for a number of specific $D \rightarrow M\gamma$ decays, grouped as Cabibbo favored, singly suppressed or doubly suppressed. In the few cases where we can employ both the above approaches, we shall refer to them respectively as ‘Meth. 1’ and ‘Meth. 2’. Given the lack of abundant $D \rightarrow MV$ data, however, we shall be forced to adopt the theoretical approach of Meth. 2 in most cases.

Before we can proceed, there is another topic which must be addressed, the dynamical complication of significant Final State Interactions (FSI). Although presumably not a problem in $B \rightarrow MV$ decays, detectable FSI are known to exist in the D -meson mass region. This can produce an ambiguity in the VMD analysis because FSI will inherently be part of any VMD amplitude obtained from $D \rightarrow MV$ data, but will not be present in the BSW construction. It is difficult to remove the effect of FSI from the phenomenological VMD amplitude because the vector meson V is to be taken off-shell, and FSI might have an important kinematic dependence, *i.e.* the p_V^2 dependence of the FSI has also to be taken into account. Consequently, any FSI effects entering in data may not be present to the same extent in the VMD amplitudes. As regards the factorization construction (Meth. 2 above), the exclusion of any FSI effects in the BSW amplitude amounts *de facto* to a specific prescription for the p_V^2 -dependence of the FSI. There is some information on the p_V^2 -dependence of the $\gamma - V$ couplings and of certain matrix elements, but it is not possible at this time to separate the two effects. As we show in the Appendix, the effect for ρ emission in $A_2(1320)$ decay can be as much as a factor of two. By contrast, no such suppression is seen in ρ -photoproduction, although in ϕ -photoproduction an effective reduction of about $\sqrt{2}$ in amplitude is observed and a somewhat smaller effect of $\sqrt{1.5}$ is seen in ω -photoproduction.

Cabibbo-favored Modes

$D^0 \rightarrow \bar{K}^{*0}\gamma$: This is an instance in which the phenomenological approach is applicable since experimental information on the $D \rightarrow MV$ intermediate state is available. There is a branching ratio determination^[6] $B_{D^0 \rightarrow \bar{K}^{*0}\rho^0} = (1.6 \pm 0.4)\%$ and the amplitude is known to be (i) almost all transverse and (ii) almost all S -wave.¹ This allows us to write the VMD contribution to $D^0 \rightarrow \bar{K}^{*0}\gamma$ as

$$\mathcal{A}_{\text{VMD}}^{\text{pv}} = \frac{e}{f_\rho} \cdot \frac{a_{D^0 \rightarrow \bar{K}^{*0}\rho^0}}{m_D E_\gamma}, \quad \mathcal{A}_{\text{VMD}}^{\text{pc}} \simeq 0, \quad (\text{Meth. 1}) \quad (66)$$

where we follow the notation of Ref. [3] and denote $a_{D^0 \rightarrow \bar{K}^{*0}\rho^0}$ as the phenomenological S -wave amplitude for $D^0 \rightarrow \bar{K}^{*0}\rho^0$. With $\Gamma_{D^0 \rightarrow \bar{K}^{*0}\rho^0} = 2.53 \times 10^{-14}$ GeV and $a_{D^0 \rightarrow \bar{K}^{*0}\rho^0} = 1.63 \times 10^{-6}$ GeV, this yields $\mathcal{A}_{\text{VMD}}^{\text{pv}}(D^0 \rightarrow \bar{K}^{*0}\gamma)$ of about 6.8×10^{-8} GeV⁻¹. The data on $D^0 \rightarrow \bar{K}^{*0}\rho^0$ is consistent with no parity-conserving (P -wave) contribution.

Alternatively, the factorization approach of Eq. (64) predicts both amplitudes. In this case, we take $a_i = a_2$, and the vector meson to be mixed with the photon is the ρ^0 , so that $V = \rho^0$ and $X = \bar{K}^{*0}$. The form factors needed are those entering in $D \rightarrow \rho$ semileptonic transitions. Making use of the measured $D \rightarrow K^*$ form factors implies $I = 1/2$. To extrapolate the form factors from $q^2 = 0$ to $q^2 = m_{K^*}^2$, we use a monopole form where the D^* is the nearest singularity. The parity-violating and parity-conserving amplitudes are given in Eq. (64) by the terms involving the A_1 and V form factors respectively. Using $f_{K^*} = 0.2$ GeV² we obtain

$$\mathcal{A}_{\text{VMD}}^{\text{pv}} = 5.1 \times 10^{-8} \text{ GeV}^{-1}, \quad \mathcal{A}_{\text{VMD}}^{\text{pc}} = 3.8 \times 10^{-8} \text{ GeV}^{-1}. \quad (\text{Meth. 2}) \quad (67)$$

We notice that $\mathcal{A}_{\text{VMD}}^{\text{pv}}$ is in reasonable agreement with the one obtained from the use of data from the nonleptonic mode, given the large uncertainties involved in these predictions. Indeed, the factorization estimate for the $D^0 \rightarrow \bar{K}^{*0}\rho^0$ S -wave amplitude gives $a_{D^0 \rightarrow \bar{K}^{*0}\rho^0} = 1.3 \times 10^{-6}$ GeV⁻¹ which is within 20% of the experimental value. It also predicts a P -wave branching fraction of 0.15% for $D^0 \rightarrow \bar{K}^{*0}\rho^0$, which is below the current upper limit of 0.30%.

¹The Particle Data Group also lists branching ratios of $(3.0 \pm 0.6)\%$ and $(2.1 \pm 0.6)\%$ for S -wave and D-wave respectively.^[6] These values are completely consistent with the fact that the total transverse mode (which must be entirely S -wave by the absence of any P -wave) is $(1.6 \pm 0.5)\%$ and that the S -wave (longitudinal) must cancel with the D-wave to produce the net zero longitudinal branching ratio.

$D_s^+ \rightarrow \rho^+ \gamma$: The VMD amplitude for this decay proceeds via $D_s^+ \rightarrow \phi \rho^+$ followed by ϕ - γ mixing. Although the branching ratio for $D_s^+ \rightarrow \phi \rho^+$ is known to be $(6.5 \pm_{1.8}^{1.6} \%)$, no information on helicities or partial waves exists, so we cannot apply the phenomenological method here. Turning instead to the factorization approach of Eq. (64), we have $X = V = \phi$ and $Y = M = \rho^+$. Therefore we require the $D_s^+ \rightarrow \phi$ semileptonic form factors evaluated at $q_0^2 = m_\rho^2$. Although there is experimental information on these decays, the branching fraction and the form factors depend strongly on $B_{D_s^+ \rightarrow \phi \pi^+}$, which is still very uncertain. Thus, again making use of $D \rightarrow K^*$ data, taking $I = 1$ and with a decay constant of $g_\rho \simeq 0.17 \text{ GeV}^2$, we find

$$\mathcal{A}_{\text{VMD}}^{\text{PV}} = 3.2 \times 10^{-8} \text{ GeV}^{-1} \quad \text{and} \quad \mathcal{A}_{\text{VMD}}^{\text{PC}} = 2.8 \times 10^{-8} \text{ GeV}^{-1} . \quad (68)$$

The Cabibbo-favored VMD amplitudes are summarized in Table 9.

Table 9 Cabibbo-favored VMD Amplitudes

Mode	$ \mathcal{A}_{\text{VMD}} \text{ (} 10^{-8} \text{ GeV}^{-1}\text{)}$	
	Parity-conserving	Parity-violating
$D^0 \rightarrow K^{*0} \gamma$	3.8	5.1-6.8
$D_s^+ \rightarrow \rho^+ \gamma$	3.2	2.8

Singly Cabibbo-suppressed Modes

$D^0 \rightarrow \rho^0 \gamma$: This process can proceed via two different intermediate states, namely $\rho^0 \phi$ and $\rho^0 \rho^0$. There is one known branching ratio $B_{D^0 \rightarrow \rho^0 \phi} = (1.9 \pm 0.5) \times 10^{-3}$ with no helicity (or partial wave) information. Letting η_T be the transverse fraction of the observed branching ratio, η_S the S -wave fraction in the transverse mode, and η_P the P -wave fraction, we then obtain for the S -wave amplitude of $D^0 \rightarrow \rho^0 \phi$,

$$a_{D^0 \rightarrow \rho^0 \phi} = m_D \sqrt{\frac{4\pi \Gamma_{D^0 \rightarrow \rho^0 \phi} \eta_T \eta_S}{|\mathbf{k}|}} = 7 \times 10^{-7} \sqrt{\eta_T \eta_S} \text{ GeV} , \quad (69)$$

and for the corresponding P -wave,

$$\frac{b_{D^0 \rightarrow \rho^0 \phi}}{m_\phi m_\rho} = \sqrt{\frac{4\pi \Gamma_{D^0 \rightarrow \rho^0 \phi} \eta_T \eta_P}{|\mathbf{k}|^3}} = 1.46 \times 10^{-6} \sqrt{\eta_T \eta_P} \text{ GeV}^{-1} , \quad (70)$$

where again we employ the notation of Ref. [3] in denoting $b_{D^0 \rightarrow \rho^0 \phi}$ as the phenomenological P -wave amplitude for $D^0 \rightarrow \rho^0 \phi$. Then, multiplying by the VMD factor e/f_ϕ , we obtain the Meth. 1 estimate

$$\mathcal{A}_{\text{VMD}}^{\text{pv}} = 0.60 \times 10^{-8} \text{ GeV}^{-1} \quad \text{and} \quad \mathcal{A}_{\text{VMD}}^{\text{pc}} = 1.0 \times 10^{-8} \text{ GeV} \quad (71)$$

for $\eta_T \sim 0.5$ and $\eta_S \sim 0.66$. On the other hand, there is no available experimental information for $D^0 \rightarrow \rho^0 \rho^0$, other than $B_{D^0 \rightarrow \pi^+ \pi^- \pi^+ \pi^-} = (8.3 \pm 0.9) \times 10^{-3}$ which can be taken as an upper limit. Let us also estimate the $D^0 \rightarrow \rho^0 \gamma$ mode in the factorization approach, which can be used to predict both the off-shell amplitudes, $D^0 \rightarrow \rho^0 \phi$ and $D^0 \rightarrow \rho^0 \rho^0$. In both cases we need the $D^0 \rightarrow \rho^0$ form factors, for which $I = 1/2$. Using Eq. (64) we obtain

$$\begin{aligned} \mathcal{A}_{\text{VMD}}^{\text{pv}}(\rho^0 \phi \rightarrow \rho^0 \gamma) &= 0.22 \times 10^{-8} \text{ GeV}^{-1} \\ \mathcal{A}_{\text{VMD}}^{\text{pc}}(\rho^0 \phi \rightarrow \rho^0 \gamma) &= 0.18 \times 10^{-8} \text{ GeV}^{-1} \\ \mathcal{A}_{\text{VMD}}^{\text{pv}}(\rho^0 \rho^0 \rightarrow \rho^0 \gamma) &= 0.75 \times 10^{-8} \text{ GeV}^{-1} \\ \mathcal{A}_{\text{VMD}}^{\text{pc}}(\rho^0 \rho^0 \rightarrow \rho^0 \gamma) &\simeq 0 \quad . \end{aligned} \quad (72)$$

Our estimate for the parity-conserving $\rho^0 \rho^0 \rightarrow \rho^0 \gamma$ transition is based on the observation that an on-shell P -wave $\rho^0 \rho^0$ state is forbidden by Bose statistics and hence the associated off-shell amplitude will be suppressed. First, let us compare the first two rows in Eq. (72) with the results obtained in Eq. (71) by making use of the $\rho^0 \phi$ data. We can see that the factorization amplitudes are lower, as caused by smaller predictions for the nonleptonic intermediate modes. In general, factorization predictions will be modified by FSI. For instance, in the case at hand there could be a large enhancement due to $K^* \bar{K}^* \rightarrow \rho^0 \phi$ rescattering effects.^[39] If this is the case, this effect strongly depends on the kinematics and it is different in the off-shell nonleptonic amplitudes entering in the calculation of the VMD diagrams. The factorization approach provides a prediction which is free from FSI effects. In these cases we will take these two estimates as the allowed range. On the other hand, factorization predicts that the $\rho^0 \rho^0$ intermediate state provides most of the VMD amplitude. When both intermediate states are taken into account in the factorization estimate, the predictions of Eq. (71) and Eq. (72) roughly agree. This will not be the case for the following mode.

$D^0 \rightarrow \phi\gamma$: Now, there is only one nonleptonic intermediate state, $\phi\rho^0$. The amplitudes as extracted from $D^0 \rightarrow \phi\rho^0$ data are

$$\begin{aligned}\mathcal{A}_{\text{VMD}}^{\text{pv}} &= \frac{e/f_\rho}{e/f_\phi} \mathcal{A}_{\text{VMD}}^{\text{pv}}|_{D^0 \rightarrow \rho^0\gamma} = 2.1 \times 10^{-8} \text{ GeV}^{-1} , \\ \mathcal{A}_{\text{VMD}}^{\text{pc}} &= 3.5 \times 10^{-8} \text{ GeV}^{-1} .\end{aligned}\quad (73)$$

On the other hand, factorization predicts the much smaller amplitudes

$$\mathcal{A}_{\text{VMD}}^{\text{pv}} = 0.7 \times 10^{-8} \text{ GeV}^{-1} \quad \text{and} \quad \mathcal{A}_{\text{VMD}}^{\text{pc}} = 0.6 \times 10^{-8} \text{ GeV}^{-1} . \quad (74)$$

Part of the difference between the predictions in Eq. (73) and Eq. (74) may be due to the presence of FSI effects in the on-shell amplitude measured and used in Eq. (73) and the assumed absence of FSI in Eq. (74). In Table 10 we include both predictions as the allowed range.

$D^0 \rightarrow \omega\gamma$: This mode is very similar to $D^0 \rightarrow \rho^0\gamma$ and we obtain from the factorization approach of Meth. 2

$$\mathcal{A}_{\text{VMD}}^{\text{pv}} = 0.7 \times 10^{-8} \text{ GeV}^{-1} \quad \text{and} \quad \mathcal{A}_{\text{VMD}}^{\text{pc}} = 0.6 \times 10^{-8} \text{ GeV}^{-1} . \quad (75)$$

$D^+ \rightarrow \rho^+\gamma$: Here, the mode $D^+ \rightarrow \rho^+\rho^0$ should give the dominant contribution to the VMD amplitude, implying the Meth. 2 amplitudes

$$\mathcal{A}_{\text{VMD}}^{\text{pc}} = 1.9 \times 10^{-8} \text{ GeV}^{-1} \quad \text{and} \quad \mathcal{A}_{\text{VMD}}^{\text{pv}} = 1.6 \times 10^{-8} \text{ GeV}^{-1} . \quad (76)$$

Incidentally, the expectation for $D^+ \rightarrow \rho^+\rho^0$ is that its branching ratio should be at least 0.4%.

$D_s^+ \rightarrow K^{*+}\gamma$: Proceeding analogously, we use the factorization estimate of $D_s^+ \rightarrow K^{*+}\rho^0$ to express the VMD amplitudes for $D_s^+ \rightarrow K^{*+}\gamma$ as

$$\begin{aligned}\mathcal{A}_{\text{VMD}}^{\text{pv}} &= \frac{e}{f_\rho} \frac{G_F}{\sqrt{2}} \frac{a_2}{\sqrt{2}} (m_{D_s} + m_{K^*}) \frac{m_\rho f_\rho}{A_1} m_{D_s} E_\gamma , \\ \mathcal{A}_{\text{VMD}}^{\text{pc}} &= \frac{m_{D_s}^3 E_\gamma}{m_{K^*} m_\rho} \mathcal{A}_{\text{VMD}}^{\text{pv}} \cdot \frac{2}{(m_{D_s} + m_{K^*})^2} \frac{V}{A_1} .\end{aligned}\quad (77)$$

Upon taking the form factors to be identical to those in $D^+ \rightarrow \bar{K}^{*0}$ in the SU(3) limit, we have

$$\mathcal{A}_{\text{VMD}}^{\text{pv}} = 1.0 \times 10^{-8} \text{ GeV}^{-1} \quad \text{and} \quad \mathcal{A}_{\text{VMD}}^{\text{pc}} = 0.9 \times 10^{-8} \text{ GeV}^{-1} . \quad (78)$$

Our VMD predictions for the magnitudes of the Cabibbo-suppressed transition amplitudes are summarized in Table 10.

Table 10 Cabibbo-suppressed VMD Amplitudes

Mode	$ \mathcal{A}_{\text{VMD}} $ (10^{-8} GeV^{-1})	
	Parity-conserving	Parity-violating
$D^+ \rightarrow \rho^+ \gamma$	1.6	1.9
$D_s^+ \rightarrow K^{*+} \gamma$	0.9	1.0
$D^0 \rightarrow \rho^0 \gamma$	0.2 – 1.0	0.5 – 1.0
$D^0 \rightarrow \omega^0 \gamma$	0.6	0.7
$D^0 \rightarrow \phi^0 \gamma$	0.6 – 3.5	0.9 – 2.1

Doubly Cabibbo-Suppressed Modes

Finally, to estimate the size of the doubly Cabibbo-suppressed modes, we consider the $D^+ \rightarrow K^{*+} \gamma$ transition. Upon computing the amplitudes using the factorization expression of Eq. (64), we obtain

$$\mathcal{A}_{\text{VMD}}^{\text{pv}} = 4.2 \times 10^{-9} \text{ GeV}^{-1} \quad \text{and} \quad \mathcal{A}_{\text{VMD}}^{\text{pc}} = 4.4 \times 10^{-9} \text{ GeV}^{-1} . \quad (79)$$

Similarly, we find for the mode $D^0 \rightarrow K^{*0} \gamma$

$$\mathcal{A}_{\text{VMD}}^{\text{pv}} = 1.75 \times 10^{-9} \text{ GeV}^{-1} \quad \text{and} \quad \mathcal{A}_{\text{VMD}}^{\text{pc}} = 1.83 \times 10^{-9} \text{ GeV}^{-1} . \quad (80)$$

5 Summary and Conclusions

The existing database for direct evidence of radiative D decays is meagre, as has been shown in Table 1. However, interesting levels of experimental sensitivity are currently being attained and we can anticipate the detection of radiative signals in the not-too-distant future. Our motivation in undertaking the study reported here has been to stimulate such experimental efforts.

As shown here, weak radiative decays of charmed mesons are not dominated by the short distance penguin diagrams of Figs. 1(a),1(c), but rather by long distance processes involving nonperturbative strong interaction dynamics. From the standpoint of probing the inner workings of the Standard Model, one might have naively hoped to use radiative charm decays in order to observe the short distance process $c \rightarrow u\gamma$. This would be in analogy with radiative B -meson decay, where the amplitude is dominated by the penguin transition $b \rightarrow s\gamma$ and receives a large enhancement from QCD radiative corrections. By contrast, the corresponding $c \rightarrow u\gamma$ charm transition is minuscule at lowest order and would require an unexpectedly large QCD enhancement to become detectable. To our knowledge, the calculation performed here of the QCD radiative correction to $c \rightarrow u\gamma$ is the first explicit and detailed analysis of this system given in the literature. In addition, we were able to employ U -spin arguments to clarify the role played by neutral, flavor-changing operators such as $\bar{u}c\bar{q}q$ which contribute to the expanded operator basis in the RG analysis. Our conclusion that the $c \rightarrow u\gamma$ QCD radiative corrections are substantially larger than for $b \rightarrow s\gamma$ is due in part to the large operator mixing at the lower renormalization scale associated with the c -quark and in part to the disparate sizes of the Wilson coefficients at the matching scale of the contributing operators. Nevertheless, the radiatively-corrected $c \rightarrow u\gamma$ penguin transition remains extremely small. The main sources of suppression are the small quark masses and also the CKM factors $|V_{cb}^*V_{ub}|^2$ occurring in the numerator of the $c \rightarrow u\gamma$ branching fraction in Eq. (26). In the Wolfenstein parameterization, with $\sin\theta_c = \lambda$, this CKM dependence amounts to a λ^{10} suppression in decay rate.

On the other hand, we have shown in Sections 3 and 4 that long distance contributions are several orders of magnitude larger. A very rough estimate of the typical branching ratio to be expected is

$$B_{D \rightarrow M\gamma} \sim \alpha_{\text{em}} B_{D \rightarrow M}^{\text{non-lept.}}, \quad (81)$$

where $B_{D \rightarrow M}^{\text{non-lept.}}$ is the branching ratio for the nonleptonic D decay to some final state M . Thus, typical branching ratios of order $B_{D \rightarrow M}^{\text{non-lept.}} \sim (0.001 - 0.05)$ would induce radiative branching ratios in the range $B_{D \rightarrow M\gamma} \sim (7 \times 10^{-6} \rightarrow 4 \times 10^{-4})$. In Sections 3 and 4 we have performed a more detailed analysis by modeling the nonperturbative dynamics.

Inspecting the long distance contributions to the set of exclusive processes $D^0 \rightarrow \rho\gamma$, $D^0 \rightarrow \omega\gamma$, $D_s \rightarrow K^{*+}\gamma$ and $D^+ \rightarrow \rho^+\gamma$ for which $c \rightarrow u\gamma$ is

the underlying transition, we see that the VMD and pole amplitudes carry a single factor λ , therefore representing an enhancement of λ^4 over the penguin amplitude. As can be seen in Table 11 the expected branching fractions for these modes are in the $10^{-6} - 10^{-4}$ range, whereas we estimate $B_{c \rightarrow u\gamma} \sim 10^{-12}$. As a consequence, $c \rightarrow u\gamma$ is not a good process to test the validity of the Standard Model. That is, a hypothetical contribution from new physics would have to be extremely large in order to overcome the long distance physics.

The situation is very different in radiative B decays. The short distance transition $b \rightarrow s\gamma$ has the same CKM structure as the corresponding long distance contributions. For instance, the mode $B \rightarrow K^*\gamma$ might conceivably have long distance contamination of the order of 20% in the rate [3]. Although this is small compared to the charm case, it would be desirable to reduce the uncertainty in the calculation of these effects in order to subtract them from the measured signal. Moreover, long distance effects could also be affecting the inclusive $b \rightarrow s\gamma$ branching ratio, therefore limiting the precision with which the Standard Model can be tested in these decays.

The various amplitudes are summarized in Table 11 and are given there in units of 10^{-8} GeV^{-1} . In principle, the most conservative attitude is to take all relative signs as unknown, which would render the calculation of branching ratios highly uncertain. Fortunately, with the aid of the quark model we can reduce this ambiguity. The relative sign of Pole-II to Pole-I contributions is affected by (i) a minus sign difference in the pole denominators, (ii) an extra minus sign in type-II amplitudes due to the vector meson propagator, and (iii) minus sign differences in the $VP\gamma$ couplings between the c -quark and light-quark EM sectors. In a quark description of a $q_1\bar{q}_2$ meson, this latter sign is inferred by studying

$$h_{VP\gamma} = e \left(\frac{q_1}{m_1} + \frac{q_2}{m_2} \right) . \quad (82)$$

Although this line of reasoning narrows down the range of predictions significantly, experimental data will be needed to obtain information regarding the relative phase between the pole and VMD contributions. In this regard, it will be helpful to note that, at least in our approach, the parity-violating amplitudes arise solely from the VMD process.

Table 11 Amplitude and Branching Fraction Predictions

Mode	\mathcal{A}^{pc}			\mathcal{A}^{pv}	$B_{D \rightarrow M\gamma} (10^{-5})$
	P-I	P-II	VMD	VMD	
$D_s^+ \rho^+ \gamma$	8.2	-1.9	± 3.2	± 2.8	6 – 38
$D^0 \bar{K}^{*0} \gamma$	5.6	-5.9	± 3.8	$\pm(5.1 - 6.8)$	7 – 12
$D_s^+ b_1^+ \gamma$	7.2	—	—	—	~ 6.3
$D_s^+ a_1^+ \gamma$	1.2	—	—	—	~ 0.2
$D_s^+ a_2^+ \gamma$	2.1	—	—	—	~ 0.01
$D^+ \rho^+ \gamma$	1.3	-0.4	± 1.6	± 1.9	2 – 6
$D^+ b_1^+ \gamma$	1.2	—	—	—	~ 3.5
$D^+ a_1^+ \gamma$	0.5	—	—	—	~ 0.04
$D^+ a_2^+ \gamma$	3.4	—	—	—	~ 0.03
$D_s^+ K^{*+} \gamma$	2.8	-0.5	± 0.9	± 1.0	0.8 – 3
$D_s^+ K_2^{*+} \gamma$	6.0	—	—	—	~ 0.2
$D^0 \rho^0 \gamma$	0.5	-0.5	$\pm(0.2 - 1.0)$	$\pm(0.6 - 1.0)$	0.1 – 0.5
$D^0 \omega^0 \gamma$	0.6	-0.7	± 0.6	± 0.7	$\simeq 0.2$
$D^0 \phi^0 \gamma$	0.7	-1.6	$\pm(0.6 - 3.5)$	$\pm(0.9 - 2.1)$	0.1 – 3.4
$D^+ K^{*+} \gamma$	0.4	-0.1	± 0.4	± 0.4	0.1 – 0.3
$D^0 K^{*0} \gamma$	0.2	-0.3	± 0.2	± 0.2	$\simeq 0.01$

Finally, let us comment on the inclusive photon spectrum. In the B system, the quark transition $b \rightarrow s\gamma$ provides a useful framework for predicting properties of the hadronic inclusive decay $B \rightarrow X_s\gamma$. Thus, one estimates the $B \rightarrow X_s\gamma$ decay rate by computing the $b \rightarrow s\gamma$ decay rate and normalizing relative to the semileptonic decays to eliminate undue dependence on the mass m_b . Likewise, one predicts the photon energy spectrum in $B \rightarrow X_s\gamma$ decay by referring to the underlying two-body $b \rightarrow s\gamma$ decay.^{[40],[41]} If quarks were free, there would be a monochromatic photon spike at $E_\gamma = (m_b^2 - m_s^2)/2m_b \simeq m_b/2$. In reality, the photon spectrum becomes broadened via hadronization of the s -quark jet. The individual strange mesons ($K^*(892)$, $K_1(1270)$, *etc*) which populate the inclusive final state X_s originate predominantly from the s -quark jet hadronization. These explanations of $B \rightarrow X_s\gamma$ inclusive decay are in accordance with the spectator model, and so isospin symmetry should manifest itself event-by-event. For example, the rates for isospin-related modes such as $B^0 \rightarrow K^{*0}\gamma$ and $B^- \rightarrow K^{*-}\gamma$

should be equal. A deviation from this pattern would constitute evidence for either non-spectator or new-physics contributions. In a heavy-quark effective theory description, such non-spectator effects would occur at subleading level.

The theoretical description of charm inclusive decay could hardly be more different. Now, there is no emergent light-quark jet which hadronizes to form the set of final states. Instead, the ‘black box’ of long-range effects such as pole-amplitudes, VMD-amplitudes, *etc* dominates the physics. Thus, to determine the photon energy spectrum in $D \rightarrow X_u \gamma$, one would sum over the most important of the exclusive radiative modes. Presumably this would yield a reasonable description at least over the part of phase space where the photon energy is largest. It would be prudent to be on the lookout for the unexpected. For example, exclusive modes in light meson radiative decay are known to exhibit rather large isospin-violating effects, as in

$$\frac{\Gamma_{K^{*0} \rightarrow K^0 \gamma}}{\Gamma_{K^{*+} \rightarrow K^+ \gamma}} = 2.27 \pm 0.30 \quad \text{and} \quad \frac{\Gamma_{\rho^0 \rightarrow \pi^0 \gamma}}{\Gamma_{\rho^+ \rightarrow \pi^+ \gamma}} = 1.76 \pm 0.49 . \quad (83)$$

If this effect were to be maintained mode by mode in the exclusive D decays, it would lead to interesting levels of isospin violation in the inclusive decay. Of our results, Table 11 indicates that the likeliest possibility for isospin violation would appear to be in $D^0 \rightarrow \rho^0 \gamma / D^+ \rightarrow \rho^+ \gamma$.

Charm radiative decays give us the opportunity to study various aspects of long distance dynamics. We have seen that the theoretical predictions of the branching fractions are, in some cases, rather uncertain due to model dependence. Experimental information will therefore be needed to complete the theoretical picture of these decays. It is an interesting irony that the understanding gained from future observation of different D radiative decays can then be used to predict more confidently the size of such effects in B decays.

The research described in this paper was supported in part by the National Science Foundation and the Department of Energy. We gratefully acknowledge useful conversations with T.E. Browder, A. Datta, T. Rizzo, X. Tata and S. Willenbrock. We also wish to thank K.J. Moriarity for his assistance with numerical calculations.

References

- [1] *CLEO* collaboration, Phys. Rev. Lett. **71**, 674 (1993).
- [2] M.S. Alam *et al* (*CLEO* collaboration), ‘First Measurement of the Rate for the Inclusive Radiative Penguin Decay $b \rightarrow s\gamma$ ’, Cornell preprint CLNS-94-1314 (1994).
- [3] E. Golowich and S. Pakvasa, ‘Uncertainties from Long Range Effects in $B \rightarrow K^*\gamma$ ’, Phys. Rev. D (to be published).
- [4] D. Atwood and A. Soni, SLAC preprint SLAC-PUB-6635 (1994); E. Golowich and S. Pakvasa, Phys. Lett. **B205**, 393 (1988); H-Y. Cheng, Taipei preprint IP-ASTP-23-94 (1994).
- [5] *CLEO* collaboration, Phys. Rev. Lett. **72**, 1406 (1993).
- [6] Particle Data Group, L. Montanet *et al.*, Phys. Rev. **D50**, 1173 (1994).
- [7] M. Selen, talk presented at APS Meeting, Washington DC, April 1994.
- [8] J. Cumalet, in *Proceedings of the Tau-Charm Factory in the Era of B Factories and CESR*, SLAC-Report-451, ed. L.V. Beers and M.L. Perl, Stanford CA (1995)
- [9] T. Inami and C.S. Lim, Prog. Theor. Phys. **65**, 297 (1981).
- [10] N. Cabibbo and L. Maiani, Phys. Lett. **79B**, 109 (1978).
- [11] M. Ciuchini *et al.*, CERN preprint CERN-TH.7283 (1994); Nucl. Phys. **B415**, 403 (1994); Phys. Lett. **B301**, 263 (1993); G. Cella *et al.*, Phys. Lett. **B325**, 227 (1994); M. Misiak, Nucl. Phys. **B393**, 23 (1993); Phys. Lett. **B269**, 161 (1991); R. Grigjanis *et al.*, Phys. Lett. **B224**, 209 (1989).
- [12] B. Grinstein, R. Springer and M. Wise, Phys. Lett. **B202**, 128 (1988); Nucl. Phys. **B202**, 128 (1988).
- [13] A.J. Buras *et al*, Nucl. Phys. **B424**, 374 (1994).
- [14] B. Pietrzyk, ‘LEP Asymmetries and Fits of the Standard Model,’ talk presented at *29th Rencontres de Moriond: Electroweak Interactions and Unified Theories*, Meribel les Allues, France, March 1994, hep-ex/9406001.

- [15] N.G. Deshpande, *et al.*, Phys. Rev. Lett. **59**, 183 (1987); S. Bertolini, F. Borzumati, and A. Masiero, *ibid.* **59**, 180 (1987).
- [16] F.J. Gilman and M.B. Wise, Phys. Rev. **D20**, 2392 (1979); C. Dib, I. Dunietz, and F.J. Gilman, Mod. Phys. Lett. **A6**, 3573 (1991); C.O. Dib, Ph.D. thesis, SLAC-Report-364 (1990); A.J. Buras, *et al.*, Nucl. Phys. **B370**, 69 (1992); *ibid.* **B375**, 501 (1991).
- [17] W. Bernreuther, Z. Phys. **C20**, 331 (1983).
- [18] E. Golowich, Phys. Rev. **D24**, 676 (1981).
- [19] M. Wirbel, B. Stech and M. Bauer, Z. Phys. **C29**, 637 (1985); *ibid.* **C34**, 103 (1987).
- [20] M. Wirbel, Prog. in Part. and Nucl. Phys. **21**, 33 (1988).
- [21] MARK III Collaboration, Phys. Rev. Lett. **60**, 1375 (1988).
- [22] C.W. Bernard, ‘Heavy-light and light-light weak matrix elements on the lattice’, review presented at *Lattice '93*, Dallas, Oct. 12-16 (1993).
- [23] C.A. Dominguez, ‘Leptonic Decay Constants of Charm and Beauty Mesons in QCD: An Update’, invited talk presented at *Third Workshop on the Tau-Charm Factory*, Marbella, Spain (1993).
- [24] J.F. Amundson *et al*, Phys. Rev. **D47**, 3059 (1993).
- [25] J. Shigemitsu, ‘Lattice Gauge Theory: Status Report 1994’, Ohio State preprint (1994), hep-ph/9408328.
- [26] D. Acosta *et al* (CLEO Collaboration), Phys. Rev. **49**, 5690 (1994).
- [27] S. Aoki *et al* (WA75 Collaboration), Prog. Theor. Phys. **89**, 131 (1993).
- [28] J.Z. Bai *et al* (BES Collaboration), ‘A Direct Measurement of the D_s branching Fraction to $\phi\pi$ ’, SLAC-PUB-95-6747 (1995).
- [29] See Chap. VII of J.F. Donoghue, E. Golowich and B.R. Holstein, *Dynamics of the Standard Model*, Cambridge University Press (1992).
- [30] Kenneth J. Moriarity, private communication.

- [31] T.M. Aliev, E. Iltan and N.K. Pak, Phys. Lett. **B334**, 169 (1994).
- [32] P. Colangelo, F. De Fazio and G. Nardulli, Phys. Lett. **B334**, 175 (1994).
- [33] P.J. O'Donnell and Q.P. Xu, Phys. Lett. **B336**, 113 (1994).
- [34] Fayyazuddin and Riazuddin, Phys. Lett. **B337**, 189 (1994).
- [35] E. Paul, *Proc. 1981 Intl. Symp. on Lepton/Photon Interactions at High Energies*, ed. W. Pfiel (Bonn, 1981) pp. 301-333.
- [36] For example, see R. Aleksan, A. Le Yaouanc, L. Oliver, O. Pène and J.-C. Raynal, 'Critical Analysis of Theoretical Estimates for B to Light Meson Form Factors and the $B \rightarrow \Psi K(K^*)$ Data', Orsay preprint LPTHE-Orsay 94/13 (1994).
- [37] Examples of analysis of this type appear in A.N. Kamal, R.C. Verma and N. Sinha, Phys. Rev. **D43**, 843, (1991); M. Gourdin, A.N. Kamal, Y.Y. Keum and X.Y. Pham, Preprint PAR/LPTHE/94-30.
- [38] *E.g.*, see p. 1569 of Ref. [6].
- [39] See the mechanism described in J.F. Donoghue, Phys. Rev. **D33**, 1516, (1986).
- [40] A. Ali and C. Greub, Phys. Lett. **B259**, 182 (1991); Z. Phys. **C49**, 431 (1991); *ibid.* **C60**, 433 (1993).
- [41] M. Neubert, Phys. Rev. **D49**, 4623 (1994).
- [42] M. Gell-Mann, D. Sharp and W.G. Wagner, Phys. Rev. Lett. **8**, 261 (1962).

Appendix: VMD in Light-Meson Radiative Decay

The original application of VMD for analyzing hadronic radiative decays occurred in the light meson sector.^[42] In order to test the VMD method using an up-to-date database, we too shall consider (briefly) light meson radiative decays in this Appendix. As we shall see from our study of two particularly clean examples, the situation is encouraging but not uniformly so. First, we shall revisit the original arena for testing VMD, the ρ and ω decays into pion-photon final states. Then we shall analyze decays of a higher mass state, the

tensor meson $A_2^+(1320)$. We stress that in each of these cases the transition is purely electromagnetic, unlike the more complicated electroweak decays treated in the main body of the paper. Therefore, the ‘pole’ amplitudes do not occur here since there is no weak mixing, so one obtains a clean look at the VMD contribution.

Radiative Decays of the Vector Mesons ρ and ω

There are three electromagnetic P -wave decays in the $\rho - \omega$ system,

$$\omega \rightarrow \pi^0\gamma, \quad \rho^+ \rightarrow \pi^+\gamma \quad \text{and} \quad \rho^0 \rightarrow \pi^0\gamma. \quad (84)$$

In the VMD approach, these are described in terms of two electromagnetic mixing amplitudes, $\omega-\gamma$ and $\rho-\gamma$, and one strong interaction vertex, $g_{\omega\rho\pi}$.

Due to the off-shell nature of the VMD amplitudes, different momentum regions occur in the $\omega\rho\pi$ vertex for the transitions of Eq. (84). In $\omega \rightarrow \pi\gamma$, the intermediate ρ propagates at $q^2 = 0$ whereas for $\rho \rightarrow \pi\gamma$ it is the intermediate ω which propagates at $q^2 = 0$. Part of the VMD folklore built up over the years is that extrapolation of the light vector meson squared-momenta from the meson mass-shell to the photon mass-shell does not strongly affect the decay amplitude. The ratio of ρ and ω decay widths can be used to test this as follows. Recall that for the VMD description of $1^- \rightarrow 0^-\gamma$ transitions, the strong vertex $g_{\omega\rho\pi}$ is related to the decay width Γ via

$$g_{\omega\rho\pi} = \left[\frac{f^2}{e} \cdot \frac{12\pi\Gamma}{|\mathbf{q}|^3} \right]^{1/2}, \quad (85)$$

where $f \rightarrow f_\rho$ for ω decay and $f \rightarrow f_\omega$ for ρ decay. Noting that the decay momenta in $\omega \rightarrow \pi\gamma$ and $\rho \rightarrow \pi\gamma$ are almost equal, one has

$$\left| \frac{f_\omega}{f_\rho} \right| = \sqrt{\frac{\Gamma_{\omega \rightarrow \pi^0\gamma}}{\Gamma_{\rho^+ \rightarrow \pi^+\gamma}}} = 3.24 \pm 0.19, \quad (86)$$

provided the *same* strong vertex is used in each decay. In the above, we have used the charged- ρ decay width in view of its superior accuracy. The value appearing in Eq. (86) is seen to be in accord with that inferred from vector meson decay into lepton pairs (*cf* Table 1 of Ref. [3]),

$$\left| \frac{f_\omega}{f_\rho} \right| = 3.39 \pm 0.10. \quad (87)$$

Alternatively, one can use each of these radiative decays to extract determinations of $g_{\omega\rho\pi}$ as in Eq. (85), and one finds

$$g_{\omega\rho\pi} = \begin{cases} (11.73 \pm 0.35) \text{ GeV}^{-1} & (\omega \rightarrow \pi^0\gamma) \\ (12.40 \pm 0.64) \text{ GeV}^{-1} & (\rho^+ \rightarrow \pi^+\gamma) \\ (16.40 \pm 2.1) \text{ GeV}^{-1} & (\rho^0 \rightarrow \pi^0\gamma) \end{cases} . \quad (88)$$

The $\omega \rightarrow \pi^0\gamma$ and $\rho^+ \rightarrow \pi^+\gamma$ determinations are seen to be consistent within experimental error. This is significant because these decays involve different momentum extrapolations as discussed above. The larger coupling obtained from $\rho^0 \rightarrow \pi^0\gamma$ decay has substantially larger errors. We now turn to a different transition in which, if one accepts the data at face value, a non-negligible momentum dependence is present.

Decays of the Tensor Meson $A_2^+(1320)$

The meson $A_2^+(1320)$ has been observed to decay into both the $\pi\rho$ and $\pi\gamma$ modes, with branching ratios

$$B_{A_2 \rightarrow \pi\rho} = 0.701 \pm 0.027 \quad \text{and} \quad B_{A_2 \rightarrow \pi\gamma} = (2.8 \pm 0.6) \cdot 10^{-3} . \quad (89)$$

These data turn out to provide a particularly clean test of the VMD method in two respects. First, there is just a single partial wave in the final state. As a consequence, the decay rates alone can be used to test VMD without any need for polarization information of the final state particles. The occurrence of a single orbital angular momentum in the final state follows from conservation of parity and of angular momentum. Thus we have

$$\mathcal{P} : \quad + = (-)^2(-)^L \implies L = 0, 2, 4, \dots \quad (90)$$

$$\mathcal{J} : \quad |\mathbf{2}| = |\mathbf{1} + \mathbf{L}| \implies L = 1, 2, 3 \quad (91)$$

which implies that $L = 2$. In addition, of the three light vector mesons ρ, ω, ϕ , only the ρ can appear together with a pion in a final state of A_2 decay. The reason is that the decay $A_2 \rightarrow \pi V$ (V is a vector meson) proceeds through the strong interactions and conservation of G -parity forbids the $\pi\omega$ and $\pi\phi$ modes. Thus, the rho is the only light vector meson involved in the VMD determination and interference with ω or ϕ mediated processes is absent.

The amplitude for the transition $A_2^+(p) \rightarrow \pi(q)^+ \rho^0(k)$ can be written as

$$\mathcal{A}_{\pi\rho} = \frac{g_{\pi\rho}}{m_A^2} \epsilon^{\mu\nu\alpha\beta} p_\mu \epsilon_\nu^\dagger(k) q_\alpha h_{\beta\sigma}(p) q^\sigma , \quad (92)$$

where $g_{\pi\rho}$ is a dimensionless quantity and $h_{\beta\sigma}(p)$ is the spin-two polarization tensor of the A_2 . From the decay rate relation,

$$\Gamma_{A_2^+ \rightarrow \pi^+ \rho^0} = \frac{g_{\pi\rho}^2}{40\pi} \frac{\mathbf{q}_{\pi\rho}^5}{m_A^4} , \quad (93)$$

one determines a magnitude for the coupling $g_{\pi\rho}$. This can be used, in turn, to predict the radiative coupling $g_{\pi\gamma}$ via the VMD formula

$$g_{\pi\gamma}^{\text{VMD}} = \frac{e}{f_\rho} g_{\pi\rho} , \quad (94)$$

and we find

$$g_{\pi\gamma}^{\text{VMD}} = 1.99 \pm 0.06 . \quad (95)$$

Alternatively, it is possible to determine the pion-photon coupling *directly*. Analogous to Eq. (92), we can write down a gauge-invariant photon-emission transition,

$$\mathcal{A}_{\pi\gamma} = \frac{g_{\pi\gamma}}{m_A^2} \epsilon^{\mu\nu\alpha\beta} p_\mu \epsilon_\nu^\dagger(k) q_\alpha h_{\beta\sigma} q^\sigma . \quad (96)$$

Fixing the coupling $g_{\pi\gamma}$ in terms of the decay rate

$$\Gamma_{A_2^+ \rightarrow \pi^+ \gamma} = \frac{g_{\pi\gamma}^2}{40\pi} \frac{\mathbf{q}_{\pi\gamma}^5}{m_A^4} , \quad (97)$$

yields the value

$$g_{\pi\gamma}^{\text{expt}} = 0.98 \pm 0.11 . \quad (98)$$

Thus, one obtains a factor-of-2 discrepancy between the empirical amplitude and the VMD prediction, with the VMD value being the larger. Several possible explanations for the lack of agreement come to mind. Although the radiative branching ratio given in Eq. (89) has reasonably small error bars, the signal is based on only one experiment. Alternatively, there may be unexpectedly large momentum dependence in the $A_2\pi\rho$ vertex. Thus, as one proceeds from the rho mass-shell ($k^2 = m_\rho^2$) to the photon mass-shell ($k^2 = 0$), a 'softening' might occur in the VMD estimate. However, to our knowledge there is no previous evidence for such momentum dependence for the ρ extrapolation.